DELPHI Collaboration

DELPHI 2002–032 CONF 566
Sept. 2, 2002

Bose-Einstein correlations in $e^+e^- \to W^+W^-$ events

N. van Remortel, F. Verbeure
Universiteit Antwerpen, B-2610 Antwerpen, Belgium

N.J. Kjaer, J. Timmermans
CERN, European Organization for Nuclear Research, CH-1211 Geneva 23, Switzerland

N. Pukhaeva
Joint Institute for Nuclear Research, Dubna, Russian Republic
Kansas State University, Kansas, USA

Z. Metreveli, K. Seth, A. Tomaradze
Northwestern University, Evanston, USA

M. Tabidze
Institute for High Energy Physics of Tbilisi State University, Georgia

A. De Angelis, L. Vitale
Università di Trieste and INFN, Trieste,
and Università di Udine, Udine, Italy

V. Perevoztchikov
Brookhaven National Laboratory, Upton, USA

Abstract

Measurements are presented on correlations between pairs of particles from different W's in the fully hadronic decay channel $e^+e^- \to W^+W^- \to q_1\bar{q}_2q_3\bar{q}_4$. The hadronic parts of the semi-leptonic channels $e^+e^- \to W^+W^- \to q\bar{q}\ell\nu$ are used to construct a reference sample. A model independent analysis is made with two independent approaches. Both analyses lead to results which are compatible with the presence of inter-W correlations with a level of significance of more than two sigma.

Contributed Paper for ISMD 2002 (Alushta, Ukraine)

1 Introduction

The pioneering experiment of Goldhaber and collaborators [1], together with a technique applied earlier in astrophysics by Hanbury-Brown and Twiss [2] marked the start of a new type of measurements dealing with multi-particle production. Particle interferometry as it is often called, uses the quantum mechanical properties of bosons and fermions to probe the space-time picture of particle production. As a consequence of being subjected to Bose-Einstein statistics, multiplets of identical bosons are expected to be produced with smaller energy-momentum difference in phase space. Bose-Einstein Correlations (BEC) have been observed and studied in many collision environments, yet our understanding of the phenomenon is far from complete.

The $e^+e^- \to W^+W^-$ events allow a comparison of the characteristics of the W hadronic decays when both W's decay hadronically in the reaction $e^+e^- \to W^+W^- \to q_1\bar{q}_2q_3\bar{q}_4$ (often refered to as $(4q)$-mode or fully hadronic mode) with the case in which one of the W's decays leptonically in the reaction $e^+e^- \to W^+W^- \to q_1\bar{q}_2\ell\nu$ (denoted $(2q)$-mode or semi-leptonic mode for brevity). Since the distance between the W^+ and W^- decay vertices is considerably smaller than the typical hadronisation distance, their decay products are expected to overlap in space and time and identical bosons from different W's can be subject to Bose-Einstein correlations.

In the framework of the precision measurements at LEP, the interest of establishing whether there are BEC between bosons from different W's is twofold. Up to now it is not yet known to which degree particles carry information about their production source. In the fully hadronic decay of a WW event it remains unclear whether one can unambiguously assign a decay particle to either of the W bosons. This has non trivial consequences on the direct reconstruction of the W mass, where one implicitly accepts the previous assumption. The modelling of BEC in the JETSET Monte Carlo code [3, 4] is still ad-hoc, therefore one can argue whether the predicted shifts in the measured W mass [5] are reliable. It is known that these models are describing BEC inside one hadronic system, either coming from a Z-decay or from the decay of a single W, but it is unknown whether BEC are present between decay products from different W's and, if so, whether they behave similarly as BEC inside an individual hadronic system. The latter might give an indication whether the observed correlations have a strict correspondence with the string breaking history, or whether they reflect the actual freeze-out volume after hadronisation, independently of the hadronisation mechanism itself.

The search for inter-W correlations at LEP2 has been performed by means of several techniques [6–8]. In this work the approach of [8] is followed, which is largely based on ref. [9]. This approach allows, by selecting fully hadronic and semi-leptonic WW decays, to construct variables which are sensitive to inter-W Bose-Einstein correlations. The data analysed in this paper correspond to three years of data taking by the DELPHI detector [10, 11] at centre-of-mass energies ranging from 189 GeV to 209 GeV with a total integrated luminosity of 547 pb^{-1}.

The paper is organised in the following way. Section 2 briefly describes the theoretical framework of two-particle correlation functions. Sections 3 and 4 describe the particle and event selections, respectively. Section 5 describes the procedure to construct a non-correlated reference sample. The statistical properties of two-particle densities are discussed in Section 6. Results are given in Section 7. An alternative analysis whose results are consstent with the first one, is discussed in Section 8, and a discussion of the

Moriond-2001 analysis in section 9. Finally a discussion and summary is given in section 10.

2 Formalism

In the framework of the formalism described in [9] and [12], the presence of two-particle correlations is studied using two-particle inclusive densities $\rho(1,2)$ defined in terms of the momentum transfer $Q_{12} = \sqrt{-(p_1 - p_2)^2}$, where p_1, p_2 are the four-momenta of the two particles:

$$\begin{aligned} \rho(1,2) &= \frac{1}{N_{ev}} \frac{dn_{pairs}}{dQ_{12}}, \\ \int_Q \rho(1,2) dQ_{12} &= \langle n_1 (n_2 - \delta_{12}) \rangle \equiv F_2, \end{aligned} \tag{1}$$

where N_{ev} is the number of events, n_{pairs} the number of particle pairs and n_1 (n_2) the number of particles of type 1 (2). The delta function δ_{12} equals zero for non identical particles and is equal to unity for identical particle species. The second expression defines the second-order unnormalised factorial moment F_2 for full phase space. In the case of two stochastically independent hadronically decaying W's the single and two-particle inclusive densities obey the following relations:

$$\begin{aligned} \rho^{WW}(1) &= \rho^{W^+}(1) + \rho^{W^-}(1), \\ \rho^{WW}(1,2) &= \rho^{W^+}(1,2) + \rho^{W^-}(1,2) + 2\rho^{W^+}(1)\rho^{W^-}(2), \end{aligned} \tag{2}$$

where $\rho^W(1)$ is the single particle density. It is worth noticing that the two-particle density of the WW system is not equal to the sum of the two-particle densities of each W. This illustrates that higher-order inclusive densities contain redundant information from lower order densities. Therefore, it is very useful to introduce the n-particle factorial cumulant correlation functions (in short: n-particle correlation functions):

$$\begin{aligned} \rho_1(1) &= C_1(1), \\ \rho_2(1,2) &= C_1(1)C_1(2) + C_2(1,2), \\ &\vdots \end{aligned} \tag{3}$$

These functions are additive and do not contain contributions from lower orders. Remember that $\rho^{W^+}(1)\rho^{W^-}(2)$, expressed in the variable Q, is in fact an integral of the type

$$\int\int d^3p_1 d^3p_2 \rho^{W^+}(1)\rho^{W^-}(2)\delta(Q^2 + (p_1 - p_2)^2). \tag{4}$$

Therefore, its notation is simplified to $\rho_{mix}^{W^+W^-}$, all the more so because it can be experimentally constructed by pairing particles from different semi-leptonic WW decays. In

this way one ensures that the particles coming from different W's do not correlate, and $\rho_{mix}^{W^+W^-}$ truly factorises in the product of single particle densities. Keeping in mind that Eq. (2) was formulated for independent W decays, one can construct test observables to look for deviations from this assumption, indicating that particles from different W decays do correlate:

$$\Delta\rho(Q) = \rho^{WW}(Q) - 2\rho^{W}(Q) - 2\rho_{mix}^{WW}(Q), \tag{5}$$

$$D(Q) = \frac{\rho^{WW}(Q)}{2\rho^{W}(Q) + 2\rho_{mix}^{WW}(Q)}, \tag{6}$$

where a simplified notation is adopted, assuming that

$$\rho^{W^+}(1,2) = \rho^{W^-}(1,2) \equiv \rho^{W}(1,2). \tag{7}$$

Any deviation from zero of Eq. (5) or any deviation from 1 of Eq. (6) would indicate the presence of inter-W cross talk. In what follows only the distribution $D(Q)$ will be examined.

This distribution $D(Q)$ is usually fitted with an exponential parametrisation of the form:

$$D(Q) = N(1 + \Lambda e^{-RQ})(1 + \delta Q), \tag{8}$$

where Λ measures the deviation from the null-hypothesis that there are no inter-W correlations, R measures the radius of emission, N is a normalisation constant and the term $(1 + \delta Q)$ takes into account possible long–range correlations.

3 Particle selection and identification

Charged particles are selected for further analysis if they fulfill the following criteria:

- momentum bigger than 0.1 GeV/c;
- Δp/p smaller than unity;
- impact parameter with respect to the nominal interaction point less than 4 cm in the plane perpendicular to the beam and $4/\sin\theta$ cm along the beam;
- the particle is not associated with a reconstructed secondary vertex.

For neutral particles at least one of the following criteria has to be fulfilled:

- energy of the shower in the small angle EM calorimeter bigger than 0.3 GeV;
- energy of the shower in the barrel EM calorimeter bigger than 1.5 GeV;
- energy of the shower in the forward/backward EM calorimeter bigger than 0.5 GeV;
- energy of the shower in the hadronic calorimeter bigger than 1.3 GeV.

The charged particles used in the analysis of the Bose-Einstein effect are subjected to more strict selections. To compute the particle densities it is required that the information from the Time Projection Chamber (TPC) of DELPHI was used to reconstruct the track, which implies an implicit track length cut of 25 cm. Only tracks in the polar angle region between 30° and 150° and a momentum bigger than 0.2 GeV/c are used. The impact parameters in the transverse and longitudinal plane are required to be smaller than 0.4 cm and 1 cm/sinθ, respectively. These cuts reduce the fraction of secondary tracks from 10% to 5% in the single particle densities.

The resolution of the opening angle α between like-sign pairs is of the order of 0.3-0.4° for Q values below 0.5 GeV. However, the reconstruction efficiency of pairs with small opening angle decreases considerably when $\alpha \to 0$ (see Fig. 1), and a cut at $\alpha > 2.5°$ was applied in the analysis.

Particles can be identified as an electron or muon, or tagged as being a decay product of a tau lepton. Muons are tagged according to the information obtained from the muon chambers and the hadronic calorimeters. Electrons are tagged if they are associated with showers in the electromagnetic calorimeters or by dE/dx information from the TPC. Both electron and muon candidates are required to have a momentum bigger than 5 GeV/c and the total electromagnetic and hadronic energy in a cone of 10° around the candidate cannot exceed 30 GeV. A particle can not be tagged as an electron if it was already tagged as a muon before. If more lepton candidates of one flavour remain, the one with the largest $|\mathrm{p}| \times \theta_{\mathrm{iso}}$ is retained. The isolation angle θ_{iso} is calculated with respect to all charged particles with momentum greater than 1. GeV/c.

Taus can be further subdivided according to their decays. The tau can either decay to a lighter lepton flavour or to a charged hadron. In the latter case, one looks for the presence of a well isolated track with momentum bigger than 5 GeV/c for which the product of its isolation angle and its momentum must be bigger than 50°GeV/c. Again, the particle with maximum $|\mathrm{p}| \times \theta_{\mathrm{iso}}$ is retained. The last possibility is that the tau decays into more than one charged hadron. In this case one searches for a narrow jet containing less than 10 particles of which maximally 5 are charged ones. In case of multiple narrow tau jet candidates, the one with the smallest, momentum weighted, angular spread is retained.

4 Event selection

4.1 Fully hadronic events

Fully hadronic events are essentially characterised by a large visible energy and a topology of four or more energetic jets.

A feed-forward neural network is used to improve the selection quality. The network is based on the JETNET package [13], uses the standard back-propagation algorithm, and consists of three layers with 13 input nodes, 7 hidden nodes and one output node. The final neural network output for data and simulated signal and background events is shown in Fig.2. The description of the preselection cuts and input variables to the neural net can be found in [14]. All numbers concerning the fully hadronic event selection are given in Table 1: efficiency, purity, number of observed and of expected events for different values

of the cut on the neural net output value, at each of the centre-of-mass energies. Stability checks and background studies were performed by making a scan over the neural network output values shown in this table. All WW like events are taken as signal, thus including part of the ZZ events.

4.2 Semileptonic event selection

The decay channel $WW \to q\bar{q}l\nu$ is characterised by the presence of two or more hadronic jets, an isolated, energetic lepton or a narrow jet in the case of hadronic τ decays, and missing energy and momentum due to the undetected neutrino(s). All events are subjected to a first set of preselection cuts:

- more than 6 charged tracks;
- transverse energy larger than 0.25 $\sqrt{s}$;
- total energy in a cone of 30° around the beam pipe less than 30 GeV;
- absence of 2 isolated leptons of the same flavour;
- polar angle of the missing momentum between 10° and 170°;
- the total energy of all neutral particles in the event less than 0.2 $\sqrt{s}$;
- a minimum of 4 particles of which at least 1 charged particle in each jet of the hadronic system.

Since further selections are dependent on the flavour of the lepton, it is appropriate to subdivide the selections in three categories: muon events , electron events and tau events. All events passing these preselection criteria are subjected to a neural network selection, based on the MLPFIT package using a hybrid-linear BFGS method [15]. Events are passed sequentially through the muon, electron and tau selections. Each event failing a previous selection is still a candidate for the following one.

The semi-leptonic event selections, including the input parameters for the neural network, are detailed in the Appendix. The efficiencies, purities, numbers of observed and expected events, are given in Table 2.

5 Experimental construction of two-particle densities

As shown in section 2, it is possible to construct variables which test the hypothesis of independent W decays, i.e. whether there are BEC between pairs of particle from the decays of *different* W's. The two-particle density of a single W, $\rho^W(Q)$, is obtained by combining particles from the hadronic system of a semi-leptonic W decay. All particles assigned to the leptonic system are removed from the calculation. Depending on the chosen value of the neural network output parameter, the fully hadronic W events can be contaminated by a considerable fraction of high energy $\mathrm{q\bar{q}}$ events. Therefore, the density $\rho^{WW}(Q)$ is corrected for this background by

energy	nnout cut	-0.3	0.0	0.3	0.6	0.9
189 GeV	eff	0.83	0.80	0.75	0.65	0.31
	pur	0.82	0.85	0.87	0.91	0.96
	obs	1345	1249	1119	956	446
	exp	1350.0	1247.6	1130.4	953.6	434.4
192 GeV	eff	0.81	0.78	0.73	0.64	0.31
	pur	0.82	0.85	0.88	0.92	0.96
	obs	227	207	183	151	68
	exp	217.7	201.4	182.8	154.6	70.8
196 GeV	eff	0.83	0.78	0.70	0.58	0.25
	pur	0.85	0.89	0.92	0.93	0.97
	obs	680	601	504	411	166
	exp	661.1	595.9	519.7	424.7	172.8
200 GeV	eff	0.80	0.77	0.72	0.63	0.30
	pur	0.84	0.87	0.89	0.93	0.97
	obs	762	695	625	504	256
	exp	718.5	666.6	606.7	514.7	236.7
202 GeV	eff	0.78	0.75	0.70	0.62	0.30
	pur	0.84	0.87	0.89	0.92	0.97
	obs	370	338	300	246	134
	exp	344.8	319.5	290.6	246.1	113.0
$>$ 202 GeV	eff	0.82	0.78	0.74	0.64	0.31
	pur	0.87	0.90	0.92	0.94	0.97
	obs	1568	1420	1239	960	494
	exp	1392.9	1299.4	1188.5	1015.4	471.9
Total number observed		4952	4510	3970	3228	1564
Total number expected		4685.0	4330.4	3918.7	3309.1	1499.6

Table 1: Efficiencies, purities, number of observed and of expexted events for the fully hadronic event selection for five cuts on the neural network output parameter.

energy	flavour	$q\bar{q}\mu\nu$	$q\bar{q}e\nu$	$q\bar{q}\tau\nu$	$q\bar{q}l\nu$
189 GeV	eff	-	-	-	0.62
	pur	-	-	-	0.97
	obs	332	264	156	752
	exp	352.0	279.1	149.2	780.3
192 GeV	eff	-	-	-	0.61
	pur	-	-	-	0.97
	obs	54	42	27	123
	exp	56.2	44.3	23.8	124.3
196 GeV	eff	-	-	-	0.64
	pur	-	-	-	0.97
	obs	174	145	74	393
	exp	172.6	136.0	72.8	381.4
200 GeV	eff	-	-	-	0.60
	pur	-	-	-	0.97
	obs	195	149	83	427
	exp	191.1	151.9	80.9	423.9
202 GeV	eff	-	-	-	0.58
	pur	-	-	-	0.97
	obs	93	85	29	207
	exp	91.0	72.2	38.5	201.7
$>$ 202 GeV	eff	-	-	-	0.61
	pur	-	-	-	0.98
	obs	320	263	144	727
	exp	359.2	284.4	149.9	793.5
Total number observed		1168	948	513	2629
Total number expected		1222.1	967.9	515.1	2705.1

Table 2: Efficiencies, purities, number of observed and of expexted events for the semi-leptonic event selections.

$$\rho^{WW}(Q) = \frac{1}{N_{tot} - N_{q\bar{q}}} \left(\frac{dn_{tot}}{dQ} - \frac{dn_{q\bar{q}}}{dQ} \right), \tag{9}$$

where N_{tot} and $N_{q\bar{q}}$ are the total number of selected events and the number of selected background events, respectively, and n_{tot} and $n_{q\bar{q}}$ the respective number of particle pairs from these events. The background is subtracted using simulated Monte Carlo events including Bose-Einstein correlations. A systematic uncertainty is assigned due to this subtraction procedure and is discussed later.
The density of mixed pairs, $\rho^{WW}_{mix}(Q)$ should approximate $\rho^{WW}(Q)$ as closely as possible with the restriction that no Bose-Einstein correlation is possible between combinations of particles coming from different W's. This is realised by definition since both particles forming a pair originate from a different event. Many ways of mixing single W decays are possible. The method used in this analysis is the following. One starts with a *pool* of selected semi-leptonic WW decays where all particles coming from the leptonic decay of one of the W's are removed. For this the tagged lepton or leptonic jet is removed, together with any possible remaining neutral particles in a cone of 10° around it. The W four-momenta are obtained from a 3C fit where energy and momentum are conserved and where every W has the nominal W mass of 80.35 GeV/c^2. The momenta were smeared in order to obtain a good description of the missing momentum spectra (see section 7.2.1). In order to make the combined event back-to-back, all particles from one W system are rotated in such a way that the directions of the momenta of the two W systems are opposite. In order to respect the polar asymmetry of the detector, two events are combined only if the W momenta are lying on a double cone or sandtimer shape with a thickness of 10°. This requirement is sketched in Fig. 3. In order to make the combined event balanced in momenta, only rotations in azimuthal angle are performed in combination with an inversion of the z component of the momenta in cases where both W directions point in the same hemisphere. This reflects the azimuthal and left-right symmetry of the detector. The remaining imbalance in polar angle is not compensated for. This mixing procedure results in a new pool of events that have the same fundamental properties as fully hadronic WW events. In order to ensure a more accurate description of the selected WW events, the same event selection is made on these constructed events as was done to select the fully hadronic events from the data. Only the events which pass this selection are considered to construct $\rho^{WW}_{mix}(Q)$. When $\rho^{WW}_{mix}(Q)$ is constructed all particle combinations coming from the same hadronic system are omitted, they are already contained in $\rho^{W}(Q)$. In some rare cases it can occur that a semileptonic event from our original mixing pool was never a good candidate to combine with to construct a mixed event. In this case the particle pairs from this event are removed from $\rho^{W}(Q)$. However, the infuence of this is very small for pool sizes of typically 100 events. From the total selected sample of semileptonic events, 96% are being used to construct $\rho^{WW}_{mix}(Q)$, resulting in a sample of 9570 mixed events.

6 Statistical properties of two-particle densities

By taking combinations of n identically charged particles one obtains a total amount of $n(n-1)/2$ entries in the density distributions. This means that a particle can have several

entries in the same bin or in different bins of the density distribution, thus introducing bin-to-bin correlations [16]. In addition, the value of n is fluctuating from event to event. In order to know the statistical bin error of the density distributions, several techniques can be applied. The simplest is a Monte Carlo resampling technique in which the analysis is repeated on N samples, containing a comparable amount of events as the data sample. This corresponds to a set of N repeated experiments. The spread on the number of bin entries for this set of N experiments gives an approximation for the true bin error, but no information on the correlation between the bins.

A more rigorous method is the calculation of the covariance matrix of the distribution [17]:

$$V_{j,k} = \frac{1}{N_{ev}-1}\sum_{i=1}^{N_{ev}}(h_j^i - H_j/N_{ev})(h_k^i - H_k/N_{ev}), \tag{10}$$

where the h_j^i are the numbers of entries in bin j of event i and $H_j = \sum_i h_j^i$. Note that the diagonal elements of the covariance matrix are the variances of each bin: $V_{i,i} = \sigma_i^2$. If operations are done on several distributions, i.e. to construct variables $D(Q)$ and $\Delta\rho(Q)$, the covariance matrices of these quantities are computed using an analytical propagation according to classical statistical methods. The covariance matrix is able to describe exactly the statistical properties of all two-particle densities, except the $\rho_{mix}^{WW}(Q)$ distribution. The reason is that the mixed events used to construct $\rho_{mix}^{WW}(Q)$ are not statistically independent. Therefore, other techniques (like resampling) have to be applied. Since a resampling method is quite time consuming and needs many Monte Carlo samples, the so called Jackknife [18] method is a very useful alternative. The Jackknife method is in principle a resampling method on the data itself, obtained by removing one observation at a time, thus investigating the statistical influence of each elementary piece of information. This means that for a sample of observations $X = (x_1, x_2, ..., x_n)$ and an estimator $\theta = f(X)$ one can construct n Jackknife samples of the form:

$$X_{(i)} = (x_1, x_2, ..., x_{i-1}, x_{i+1}, ..., x_n). \tag{11}$$

In this case $f(X_{(i)})$ is called the i-th Jackknife replication of θ, with an average value of

$$\bar{\theta} = \sum_{i=1,n} \theta_i/n. \tag{12}$$

The Jackknife estimate of the standard error on $\bar{\theta}$ is then defined as

$$\sigma_{Jack} = \sqrt{\frac{n-1}{n}\sum_{i=1,n}(\theta_i - \bar{\theta})^2}. \tag{13}$$

The results with the Jackknife method were found to be in agreement with the diagonal elements of the covariance matrix and errors obtained by resampling for the $\rho^{WW}(Q)$ and $\rho^{W}(Q)$ distributions. A comparison of different error estimates for the $\rho_{mix}^{WW}(Q)$ distibution

is shown in Fig. 4 for a random event sample of 330 semileptonic events used to construct 5800 mixed events. Fig. 4 shows that the covariance matrix underestimates the statistical errors of $\rho_{mix}^{WW}(Q)$ drastically. The Jackknife method gives an accurate description of the statistical error in the Q region below 1 GeV, whereas at larger Q-values it overestimates the statistical error by 30 to 40 %. Since the low Q region dominates the errors on our measurements, it was found sufficient to apply the Jackknife method in order to obtain correct statistical errors for $\rho_{mix}^{WW}(Q)$. For all other two-particle densities the covariance matrix approach was chosen.

7 Results

The analysis focusses on the $D(Q)$ variable from Eq. 6, constructed as described in sections 2 and 5. All statistical uncertainties are computed according to section 6. The distribution $D(Q)$ is fitted with Eq. 8, where the radius R is fixed to 0.82 fm, as measured for the BEfull sample. The BEfull sample is a Monte Carlo sample of events where BEC are allowed between all like-sign bosons, including bosons originating from different W's.

In every case the fit range is taken between 0 and 4 GeV/c^2. The background fraction of high energy $q\bar{q}$ events was subtracted using a total of 300k simulated MC events, equally divided over the 6 energy points. They are generated with the KK2F generator, including the LUBOEI(BE_{32}) model with parameter settings PARJ(92)=0.9 and PARJ(93)=0.34. The values of the fitted parameters to the combined data set from 189 to 209 GeV are shown in Table 3 for different neural network cuts of the ($4q$) sample. All indicated errors are statistical only.

nn cut/parameter	Λ	δ	N	χ^2 (97 NDF)
-0.3	0.118 ± 0.046	0.0031 ± 0.0070	0.965 ± 0.028	76.0
0.0	0.125 ± 0.046	0.0032 ± 0.0070	0.970 ± 0.028	77.1
0.3	0.146 ± 0.047	0.0033 ± 0.0072	0.974 ± 0.029	71.1
0.6	0.142 ± 0.049	0.0025 ± 0.0074	0.986 ± 0.031	66.4
0.9	0.161 ± 0.061	-0.0001 ± 0.0092	0.992 ± 0.039	72.8

Table 3: Results of the fit of $D(Q)$ to Eq. 8, for different values of the cut on the neural net output parameter in the ($4q$) sample, and with a cut on the opening angle α between pairs larger than 2.5° (see section 7.2.4).

7.1 Systematics

Several systematic cross-checks were performed using a set of Monte Carlo events where only correlations between particles coming from the same W were allowed (called the BEins sample). A total of 350k events were generated with WPHACT, using the same BE_{32} model with PARJ(92)=1.35, again equally distributed over all energies. It will be shown later that fits to this MC set, having only correlations inside the same W cover the bulk of the systematic uncertainties. For both the BEins and the BEfull samples, the gaussian parametrisation of LUBOEI was used. The values of the fitted parameters

to the combined data set from 189-209 GeV for the BEins sample are shown in Table 4, third column.

The uncertainty in the background shape was addressed in the following way. The LUBOEI parametrisation is tuned using data from Z calibration runs. The model with parameter PARJ(92)=1.35 described best the total hadronic Z sample as can be seen in Fig. 5 and 6. However, when selecting 4 jet events this description becomes worse when going to bigger jet resolution values, corresponding to well separated 4 jet events. This subclass of events is best described with a tuning using PARJ(92)=0.9. Since it is more likely that the selected high energy $q\bar{q}$ background is of the 4 jet type, we use the latter tuning as standard background tuning. A systematic study was performed, subtracting background where half of the events had a value of PARJ(92)=0.9 and half a value of 1.35. The deviation from the nominal data value was taken as systematic uncertainty due to the background shape. In Table 4, the statistical error on the Λ-value of the data, two dominant systematic uncertainties on the Λ parameter and the resulting total error are summarised for all neural network output cuts used.

nn cut	stat. error	Λ BE ins	*Background*	total
-0.3	0.046	0.012±0.007	0.026	0.054
0.0	0.046	0.013±0.007	0.020	0.052
0.3	0.047	0.013±0.007	0.014	0.051
0.6	0.049	0.012±0.007	0.009	0.051
0.9	0.061	0.012±0.009	0.002	0.062

Table 4: Statisical error on the Λ-value on the data sample, systematic error from the BEins Monte Carlo sample, systematic error from the background subtraction and combined error, for different values of cuts on the NN output.

This study shows that the combined error is smallest for neural network cuts between 0.3 and 0.6. From those two points the neural network cut at 0.6 was chosen as standard working point, having the lowest background uncertainty of these three options. From now on, all further studies will be performed using this neural network output cut.

7.2 Cross-checks and stability

The analysis was subjected to a series of tests in order to check its stability and performance. Furthermore, individual components of possible systematic bias, studied by means of the LUBOEI BEins Monte Carlo, were investigated and proven to be small.

7.2.1 Event shapes and single particle spectra

In order to check whether the mixed semileptonic events approach as much as possible the physical properties of real fully hadronic events, a large number of event shapes and single particle distributions of the $(4q)$ sample and of the mixed sample were compared. All event shapes used as input for the neural network selection of the fully hadronic sample are compared in Fig. 7. for the BEins Monte Carlo sample at 189 GeV. The comparison of the $(4q)$ real data at 189 GeV with the mixed events is shown in Fig. 8.The fully hadronic neural network selection includes the following input variables.

1. The difference between the maximum and minimum jet energy after a 4C fit, imposing momentum and energy conservation;
2. the effective centre of mass energy $\sqrt{s'}$;
3. the value of y_{34} from the DURHAM [19] clustering algorithm;
4. the minimum angle between two jets after the 4C fit;
5. the sphericity;
6. the thrust value;
7. the minimum jet broadening B_{min};
8. the minimum jet multiplicity ;
9. the Fox-Wolfram moment H3 [20];
10. the Fox-Wolfram moment H4;
11. the maximum probability for all jet pairings, derived from the χ^2 of a 6C fit, requiring the two di-jet systems to have the same mass, equal to the nominal W mass.
12. the total transverse energy;
13. the total charged energy;

    All above variables are scaled such that their values are in the range from 0 to 1. To this, a set of five other useful variables was added:

14. the charge multiplicity;
15. the amount of missing momentum;
16. the $D_{4C} = \frac{E_{min}}{E_{max}} \frac{\theta_{min}}{E_{max}-E_{min}}$ variable;
17. the number of natural jets, clustered with LUCLUS, using a resolution variable $d_{join} = 6.5$;
18. the neural net output variable.

Some relevant single particle spectra such as the momentum, transverse momentum and rapidity w.r.t. to the thrust axis and the polar angle of all charged particles used to construct the two-particle densities are compared in Figs. 9 and 10 for Monte Carlo BEins and for data, respectively. In general a very good agreement between fully hadronic events and mixed semileptonic events was found over all years in data and MC. Any disagreements between the real 4 quark sample and the mixed events indicate possible flaws in the mixing method. The influence of these discrepancies was tested in two ways. Taking the W direction obtained from the constrained fit when mixing two semileptonic events results in a missing momentum distribution shown on the left hand side of Fig. refpmisprob. This discrepancy can be reduced by taking a linear combination of the fitted W direction and

the sum of momenta of all particles assigned to the hadronic W system. When using this information in the mixing procedure, the distribution on the right hand side in Fig. 11 is obtained. The last procedure was used as default. The $D(Q)$ distribution was fitted with Eq. 8 for both procedures using a MC sample at 189 GeV. The difference in fitted Λ parameters gives an indication of the systematic uncertainty due to imperfect mixing. This difference amounted to

$$\Delta\Lambda_{pmiss} = \Lambda(default) - \Lambda(pmiss) = 0.005. \tag{14}$$

The second way to investigate the influence of discrepancies is to reweight mixed events in order to get a perfect agreement with the selected ($4q$) events. Weights were calculated for the first neural network input variable, where the discrepancy was largest (see Fig. 7) and applied to the mixed events for the same MC at 189 GeV. The difference between the default analysis was again taken as systematic uncertainty:

$$\Delta\Lambda_{weight} = \Lambda(default) - \Lambda(weight) = 0.005, \tag{15}$$

thus indicating that both approaches give a similar result.

7.2.2 Event selections

Strict event selections have the advantage that the background uncertainty is highly reduced. On the other hand they can bias the two-particle densities, i.e. it is obvious that if one requires a WW event with well separated jets, that the two-particle density for tracks coming from different W's will be influenced. Therefore, the two particle efficiencies in the variable Q were checked for both the fully-hadronic and semi-leptonic event selections, based on the MC sample BEins, defined as:

$$\epsilon = \frac{\rho(Q)_{selected}}{\rho(Q)_{signal}}. \tag{16}$$

The efficiencies for the fully hadronic selection are shown on the left hand side of Fig. 12, both for particle pairs coming from the same and from different W's. The efficiencies of the semileptonic event selection and the fully hadronic selection on mixed pairs are shown on the right hand side in Fig. 12. The particle pairs inside a single W are not affected by the selections, while the pairs from different W's are affected, but in a similar way for fully hadronic events as in mixed events. In order to estimate the size of the overall bias on the measurement due to the event selection, all two-particle spectra were corrected with their corresponding efficiencies. The difference between the fit to the nominal BEins sample at 189 GeV and the corrected sample amounted to:

$$\Delta\Lambda_{selection} = \Lambda(default) - \Lambda(corrected) = 0.010. \tag{17}$$

7.2.3 Lepton flavour dependence

As was discussed in section 3, the semileptonic event selection depends on the lepton flavour. It is investigated how much the reference sample, being the denominator of Eq. 6, depends on the semi-leptonic selections for each flavour. The hadronic part of the event, which is used to construct the reference sample, should in principle not depend

on the lepton flavour, but practice shows that identification and removal of tau jets and electrons is more problematic than muons. The analysis is therefore performed using either only mixed muon events, or electron events or tau events. The mixed samples were compared, making the following ratio's:

$$bias_{lepton} = \frac{2\rho^W(Q)_f + 2\rho^{WW}_{mix}(Q)_f}{2\rho^W(Q)_{f'} + 2\rho^{WW}_{mix}(Q)_{f'}}, \tag{18}$$

where f and f' denote two different lepton flavour selections. The obtained ratio was fitted with Eq. 8, fixing the radius to 0.75 fm. The results of this fit are:

$$\begin{aligned} \Lambda\text{bias}_{e/\mu} &= 0.002 \pm 0.012 \\ \Lambda\text{bias}_{e/\tau} &= -0.022 \pm 0.015 \\ \Lambda\text{bias}_{\mu/\tau} &= -0.026 \pm 0.015 \end{aligned} \tag{19}$$

The different biases are shown in Fig. 13.

7.3 Results of this analysis

WW-events, both fully hadronic and semi-leptonic, were selected using a neural network algorithm. Taking into account the dominant systematic uncertainties, an optimal working point was found for the selection of fully hadronic events. This point corresponds to a cut on the fully hadronic neural net output at 0.6. Moreover, a cut on the opening angle between pairs ($\alpha > 2.5^\circ$) was applied. Cross-checks and stability checks were made using a Monte Carlo sample of WW's where BEC were present between bosons from the same W (BEins sample). Comparison of the experimental results is also made with a Monte Carlo sample where BEC are allowed between all bosons, including the decay products from different W's (BEfull).

The $D(Q)$ distributions for data, the BEins model and the BEfull model, are shown in Fig. 13 The fit results for the data and both MC models are summarised in Table 5 and Table 6 for like-sign and unlike-sign particle pairs, respectively. The results given are obtained using the diagonal elements of the covariance matrix. The influence of the full correlation has been studied and the variation of the result is expected to be around 25% of the quoted error. Therefore these results remain preliminary until the optimal full correlation treatment is applied for the final results. The errors and χ^2 from the results have been verified with resampling techniques. However, some care must be taken in the next section, where some parameters are different and the comparison of errors have not been verified to a precision better than 10%.

The column in Table 5 with the results from the data show that there is a 2.8σ effect of Bose-Einstein correlations between bosons from *different* W's, combining the statistical and systematic errors in quadrature. The Λ-value of the data is 1.9σ below the one of the model with full BEC. Table 6 shows that BEC between bosons from different W's also introduce an effect, though smaller, in the unlike-sign bosons in the Monte Carlo model BEfull, and that the magnitude is the same for the data and the Monte Carlo.

Fig. 15 shows the Λ–values obtained at all energies considered and the value obtained with the combined sample. Finally, as a test of the stability of the results as a function of the purity of the sample, Fig. 16 shows the Λ-value as a function of the neural net output variable, from -0.3 to 0.9, corresponding to purities of the fully hadronic WW sample

parameter	data	data R free	BE ins	BE full
Λ	0.142±0.049 (stat) ±0.015 (syst)	0.257±0.158	0.012±0.007	0.241±0.009
R (fm)	0.82 (fixed)	1.50±0.76	0.82 (fixed)	0.822±0.031
δ	0.0025±0.0074	0.0002±0.0004	-0.0013±0.0007	0.0051±0.0007
N	0.986±0.031	0.992±0.008	0.995±0.002	0.967±0.003
χ^2 (97 DF)	66.4	65.4	64.9	179.8

Table 5: Fitted parameters for data and MC predictions of the $D(Q)$ variable for like-sign particle pairs. All errors are statistical only, unless indicated.

parameter	data	BE ins	BE full
Λ	0.109±0.045	0.010±0.007	0.092±0.005
R (fm)	0.82 (fixed)	0.82 (fixed)	0.82 (fixed)
δ	0.0052±0.0074	-0.0002±0.0007	-0.0007± 0.0004
N	0.982±0.030	0.995±0.001	0.984±0.001
χ^2	73.0	87.6	186.9

Table 6: Same as in Table 5, but for unlike-sign particle pairs.

ranging from about 83% to more than 96%. At each cut on the neural net output variable, three values of Λ are shown, corresponding to no background subtraction, subtraction of background using PARJ(92)=0.9 (the standard background sample) and one using half of the sample with 0.9 and half with 1.35 as input parameter to the Monte Carlo. Fig. 16 shows that the background subtraction has only a small influence on the determination of Λ, particularly at the working point with the cut on neural network output parameter equal to 0.6, and that the final value of the analysis

$$\Lambda = 0.142 \pm 0.049 \text{ (stat)} \pm 0.015 \text{ (syst)} \tag{20}$$

is compatible within a fraction of the statistical error with the Λ-value extrapolated to zero background in the plot of Fig. 16.

8 An alternative analysis

An alternative analysis was made, using a different event selection and mixing method. The event selections were based on sequential cuts and were similar to those in [21], yielding for the fully hadronic sample a purity and efficiency of 90% and 54%, respectively. The most important selection pertained to the cut D_{4C} >0.006 rad.GeV^{-1}, with D_{4C} defined in section 7.2.1 (variable 16). The corresponding numbers for the semileptonic channel were 96% and 50%. The numbers of events selected (expected) for the fully hadronic and semileptonic channel were 2807 (2792) and 2233 (2326), respectively. The same strict requirements for the track selections were used to enhance the fraction of directly produced particles subject to BEC, as in the above analysis.

The correlation functions for fully hadronic and semileptonic channels, $R_{4q}(Q)$ and $R_{2q}(Q)$, defined as the ratio of the Q-distributions for data and simulated events (with-

out BEC included), are shown in fig. 17aand 17b for like–sign and unlike–sign pairs, respectively.

Averaged over all energies, the selected WW fully hadronic events contained 10% of $q\overline{q}$ events. The correction for these background contributions to the fully hadronic sample was done in the following way. A sample of $q\overline{q}$ events was generated with BEC included according to LUBOEI BE_{32} with parameters λ=1.35 and r=0.58 fm as was tuned at the Z-peak. These events were subjected to the same event and track selection criteria as the fully hadronic sample and the Q-distribution of the background was calculated from the events passing the selection. The agreement between data and simulated events at the Z-peak for 4 jet samples selected using the d_{join} requirement was then checked. The agreement for all events is satisfactory, while the model strongly overestimates the correlations at low-Q for selected 4 jet samples. Correspondingly, another simulated sample at the Z-peak was also used, with reduced parameter of λ=0.90 (instead of λ=1.35). Good agreement between data and these simulated events was found at the Z-peak for 4 jet samples.

The Q plot for simulated background $q\overline{q}$ events was corrected for the discrepancy between the Z-peak data and the corresponding simulated sample after 4 jet selections. This distribution, properly weighted by the percentage of the background, was subtracted from the experimental WW (4q) distribution. Alternatively, the contribution of background $q\overline{q}$ events was subtracted using the simulated sample with parameter λ=0.90 (without corrections). These two procedures yielded practically the same background subtracted distributions, yielding a difference in Λ–value of 0.004 only.

The Q-distributions for real WW fully hadronic events and for background events, calculated as described above, are shown in figure 17c. Figure 17d presents the $R(Q)$ distributions for WW (4q) events without (closed circles) and with background subtraction (open circles). The background contribution practically does not change the Q-distribution for (4q) events. In the subsequent analysis the $R(Q)$ distributions after the background subtraction were used.

To perform a direct measurement sensitive to BEC between particles from different W's, the analysis used a comparison sample which contained only BEC for particle pairs coming from a single W boson, but not for particle pairs from different W's. This comparison sample of $(4q)$-like events was constructed by the mixing of two hadronic W's from different $(2q)$ events in the following way.

The pairs of W's were accepted for mixing if these pairs had momentum imbalance $\mid \overrightarrow{P}_1 + \overrightarrow{P}_2 \mid < 25$ GeV/c. From each selected semileptonic event, the hadronic part was boosted to the rest frame of the W candidate. The rest frames of the W candidates were determined using the energy and momenta of the W's obtained from the kinematical fits. The mixed event was then constructed from two W candidates by boosting the particles of the individual W's in opposite directions. The boost vectors were determined taking into account energy-momentum conservation and the fitted masses of the W candidates. The fully hadronic event selections were applied to the mixed events. The event shape variables, multiplicities and single particle distributions for fully hadronic and mixed events were compared. In general good agreement was found.

The expected R_{4q} when there are no correlations between W's, constructed from the experimental values of $P_{2q} = \rho^W(Q)$ (for pairs from the same W) and from the mixed sample $P_{mix} = \rho^{WW}_{mix}(Q)$ (for pairs from different W's), can be written as

$$R_{4q}(Q)(mixing) = \frac{[2P_{2q}(Q) + 2P_{mix}(Q)]_{data}}{[2P_{2q}(Q) + 2P_{mix}(Q)]_{DELSIM\ no\ BE}}, \tag{21}$$

where $P_{mix}(Q)$ was obtained using the mixing of two $(2q)$ events as described above. The measured $R_{4q}(Q)$ and $R_{4q}(Q)(mixing)$ are shown in Fig. 18a for like-sign pairs, indicating correlations between particles from different Ws.

To perform model independent measurements of correlations between particles from different W's, the ratio :

$$D(Q) \equiv \frac{P_{4q}(Q)}{2P_{2q}(Q) + 2P_{mix}(Q)}\,, \tag{22}$$

which is independent of any Monte-Carlo model was used. This distribution was fitted by Eq. 8. The full covariance matrix was used in the fitting procedure as described in [17].

The resulting $D(Q)$ plots for like–sign particle pairs are shown in Fig. 18b. The fit for the model with full BEC gave the following results (with free λ, R, N and δ):

$$\Lambda(full\ BE) = 0.227 \pm 0.026\ \text{(stat)} \tag{23}$$

$$R(full\ BE) = 0.895 \pm 0.100\ \text{(stat) fm} \tag{24}$$

Fixing the parameter R to the value obtained above (R=0.895 fm) and repeating the fit for the model with inside BEC and for the data (with free λ, N and δ), yielded

$$\Lambda(inside\ BE) = -0.002 \pm 0.016\ \text{(stat)} \tag{25}$$

for the model with inside W's BEC, and

$$\Lambda(data) = 0.149 \pm 0.045\ \text{(stat)}\ ^{+0.025}_{-0.020}\ \text{(syst)} \tag{26}$$

for data after background subtraction.

The systematic error quoted on the measured value of $\Lambda(data)$ in Eq. 26 is the sum in quadrature of the following contributions.

– Due to the event mixing technique. Two estimates were made.

  The model with BEC only inside W's should give Λ=0.0. The magnitude of the value $\Lambda(inside\ BE)$ plus one sigma (Eq. 25) is 0.018.

  The effects of discrepancies between fully hadronic and mixed events were studied. Weights were assigned to the mixed events which were equal to the ratio of the event shape and single particle distribution variables. The maximum deviation obtained from the value (Eq. 26) was 0.020.

  The value $\pm$0.020, i.e. the larger of these two estimates, was used as a conservative systematic error due to the mixing technique.

– Due to background events. The value of the parameter $\Lambda(data)$ without background subtraction was

$$\Lambda(data) = 0.164 \pm 0.043\ \text{(stat)}\,. \tag{27}$$

  The difference between the values of Eq. 26 and Eq. 27, i.e. +0.015, was used as an estimate of this systematic error.

– The contribution due to other sources was found to be negligible.

The analysis was repeated using the requirement $\alpha > 3^\circ$, where α is the angle between pairs of particles. The fit for the prediction of the model with full BEC gave:

$$\Lambda(full\ BE, \alpha\ cut) = 0.292 \pm 0.037\ (\text{stat}) \tag{28}$$

The $\alpha > 3^\circ$ requirement increases the Λ value but not the sensitivity to inter-W correlations if the latter is defined as the Λ-value divided by its error.

The fit values for the prediction of the model with inside BEC and for the data were

$$\Lambda(inside\ BE, \alpha\ cut) = -0.002 \pm 0.021\ (\text{stat})\,, \tag{29}$$

$$\Lambda(data, \alpha\ cut) = 0.177 \pm 0.055\ (\text{stat})^{+0.033}_{-0.023}\ (\text{syst})\,. \tag{30}$$

A similar analysis was performed for unlike–sign particle pairs. The measured $R_{4q}(Q)$ and $R_{4q}(Q)(mixing)$ are shown in fig. 18c for unlike-sign pairs, indicating also the existence of correlations between unlike–sign particles from different W's.

The resulting $D(Q)$ plots for unlike–sign particles are shown in Fig. 18d. The fit for the model with full BEC (with free Λ, R, N and δ) gave:

$$\Lambda_{+-}(full\ BE) = 0.067 \pm 0.014\ (\text{stat}) \tag{31}$$

$$R_{+-}(full\ BE) = 0.338 \pm 0.086\ (\text{stat})\ \ \text{fm} \tag{32}$$

Fixing the parameter R to the value obtained above (R=0.338 fm) and repeating the fit for the model with inside BEC and for the data (with free Λ, N and δ), yielded

$$\Lambda_{+-}(inside\ BE) = -0.007 \pm 0.012\ (\text{stat}) \tag{33}$$

for the model with inside W's BEC only, and

$$\Lambda_{+-}(data) = 0.079 \pm 0.036\ (\text{stat})\ ^{+0.025}_{-0.019}\ (\text{syst}) \tag{34}$$

for the data after background subtraction. (The index $+-$ for fitted parameters of unlike–sign particle pairs is used to distinguish them from those of like–sign pairs).

Summarising this independent analysis, evidence for inter-W BEC is found at a level of significance of 3.0σ. The measured Λ-value is lower than the one of the model with full BEC by 1.4σ. The Λ_{+-} values for the data and for the model with full BEC are fully compatible (Eqs. 31 and 34).

The observation of correlations between like-sign particle pairs alone does not insure that the observed correlations owe their origin to Bose-Einstein correlations. They could, for example, arise from final state interactions between pions with small relative momenta. It turns out that it is possible to discount the latter possibility by virtue of the smaller correlations between unlike-sign pions, which could arise from final state interaction effects. As was shown, the unlike-sign pairs show also a correlations. The like-sign pions necessarily are in an isospin I=2 state and the unlike-sign pions are dominantly in the

isospin I=0 state. The scattering length for I=2 is more than a factor three smaller than the one for I=0 [22]. This insures that the final state interaction effects for like-sign pion pairs are expected to be nearly an order of magnitude smaller than those observed in unlike-sign pions. Even if one would attribute all the correlations observed for unlike-sign pions to final state effects, then essentially none of the correlation effects observed in like-sign pairs can therefore be attributed to final state interactions.

On the other hand, it is known that at LEP energies for high multiplicity events, as well as a clear effect on like–sign particle correlations, the BEC affect unlike–sign particle pairs as well. These so-called 'residual BEC', discussed in details in [23], were observed at Z energies by three LEP experiments [25–28]. The results presented here indicate that such correlations take also place for particle pairs from different W's. The influence of BEC to unlike–sign particles is also predicted by LUBOEI (see [25, 29]), and by a 'reweigthing' BEC model [23]. From generalised Bose statistics and isospin invariance follows also that pairs with different charges which belong to the same isospin multiplet may show a BEC enhancement [24].

Thus, one may conclude that the observed correlations between particles from different W's for like-sign as well for unlike-sign particle pairs can be ascribed to BEC.

9 Differences with the Moriond-2001 analysis

The results of this analysis, and of the alternative one, differ from the ones presented at the Moriond 2001 conference [30]. In order to understand the differences it should be pointed out that major components of the analysis were changed.

- The selection of events was done with sequential cuts, versus a neural net selection in the actual analysis. The purity of the sample was about 83%, implying the importance of a correct background subtraction. In the actual analysis the purity is about 92%. Moreover, the statistics of semi-leptonic events increased by 20%, allowing for a larger sample of mixed events.

- The background subtraction was done using a Monte Carlo sample as described in section 7, with strength parameter PARJ(92)=1.35. As explained in section 7.1, the 4 jet $q\bar{q}$ events are better described by Monte Carlo with PAR(J(92)=0.9 used in the actual analysis.

- The mixing method differs considerably: W-momenta are now taken from a 6C-fit i.s.o. a 5C fit; only rotations in azimuth of the events are applied and events are used only if the W-momenta were lying on a diabolo (see figure 2) i.s.o. a momentum balance cut; the number of re-uses of semi-leptonic events was limited to a small number, this limitation being removed in the actual analysis. Comparison of the distributions of input variables to the neural net of the data and the mixed events (figure 8), and in particular of the single particle distributions (figure 10) show that the agreement between the real 4q data and the mixed events has considerably improved in the actual analysis compared to the Moriond 2001 one.

- A cut on the opening angle of the pairs is applied. However, it was checked that this cut does not change the Λ value in the actual analysis.

10 Summary

Data from the LEP2 running at energies between 189 and 206 GeV centre-of-mass, corresponding to an integrated luminosity of 547 pb^{-1}, collected by the DELPHI detector, have been used to investigate the possible presence of Bose-Einstein correlations between bosons from different W's in the reaction $\mathrm{e}^+\mathrm{e}^- \to \mathrm{W}^+\mathrm{W}^- \to q_1\bar{q}_2q_3\bar{q}_4$. The method used is the one proposed in [9]. The quantity $D(Q)$, defined in Eq. 6, is computed and fitted to Eq. 8. A deviation of the Λ–value from zero indicates the presence of correlations between pairs of particles from different W's. The hadronic parts of semi-leptonic decays were used to construct a reference sample by mixing techniques.

Two independent analyses were made, based on different event selections: one using a neural network to select the fully hadronic and the semi-leptonic samples, and one using sequential cuts and selections. Also the mixing technique differed in the two analyses.

The results can be summarized as follows:

- The preliminary DELPHI result for $\Lambda = 0.142 \pm 0.049(stat) \pm 0.015(syst)$;
- both analyses lead to the observation of BEC between like-sign pairs from the decays of different W's at a level of significance of more than two sigma away from the hypothesis of no inter-W correlations;
- compared with the full correlation LUBOEI model, which is currently used to estimate the systematic error on the W-mass determination, the Λ-value obtained for the data is about one and a half sigma lower;
- correlations between unlike-sign particles are also observed; in both analyses the strength of these correlations is compatible with the one expected from a Monte Carlo model which includes BEC between all like-sign bosons.

Appendix: selection of semi-leptonic events

In this appendix the details are given of the selections of semi-leptonic events, including the input data for the neural network.

1. **Muon events**

   After requiring the presence of a tagged muon, the following preselections were applied before subjecting the event to the neural network selection:

   - the momentum of the muon cannot be lower than $0.15\sqrt{s}$ if simultaneously the invariant mass of the lepton-neutrino system is lower than 60 GeV/c^2;
   - the invariant mass of the $q\bar{q}$ and of the $l\nu$ system has to be bigger than 10 GeV/c^2;
   - $p \cdot \theta_{iso} > 250°$GeV/c.

   The 9 input variables to the neural network are then:

   (a) the muon momentum;
   (b) the muon isolation angle;
   (c) the missing momentum;
   (d) $|\cos(\theta_{\mathrm{miss}})|$;
   (e) the opening angle between the muon and the missing momentum direction;
   (f) the transverse energy;
   (g) the total visible energy;
   (h) $\sqrt{s'}/\sqrt{s}$, where $\sqrt{s'}$ is the effective centre of mass energy;
   (i) the angle between the muon and the combined di-jet momentum

   The final network output is required to be bigger than 0.4. The neural network output variable for the muon selection is shown in Fig. 2. All event selection numbers for all energies and lepton flavours are shown in Table 2.

2. **Electron events**

   An event is considered as an electron event if a tagged electron is detected. The same precuts are applied to the electron candidate events, including the additional requirement that the polar angle of the electron lies between 20° and 160°. The final cut on the neural network output amounts to 0.4 as well.

3. **Tau events** The following precuts are common to both one prong tau and multi-prong tau categories:

   (a) the total visible energy less than 0.85 $\sqrt{s}$;
   (b) the effective centre of mass energy $\sqrt{s'} < \sqrt{s} -$ 10 GeV;
   (c) the polar angle of the missing momentum between 15° and 165°;
   (d) the jet separation variable y_{34} of the Durham clustering algorithm [19] has to be lower than 0.03

(e) the $\sqrt{s'}$ value cannot be lower than 105 GeV or be smaller than $\sqrt{s}-$ 25 GeV if simultaneously the missing momentum has a polar angle between 35° and 145°.

4. **Single isolated track**

   If a single isolated track is tagged, the event is rejected if the azimuthal angle between the 2 hadronic jets is bigger than 165° and if simultaneously the angle between the track and the hadronic event plane is between 83° and 97°. If the isolated track is identified as a muon or an electron the sum of the energies of all neutral tracks in a cone of 15° around the lepton can not exceed 10 GeV, otherwise it is classified in the narrow tau jet category. In addition the number of neutrals in this cone was calculated to make a further classification. If the sum of the energy of the isolated track and its surrounding neutrals is bigger than 5 GeV and if the product of this energy with the isolation angle of the track is bigger than 150°GeV a first classification is made:

   (a) tautype = 1 if the isolated track is identified as an electron

   (b) tautype = 2 if the isolated track is identified as a muon

   (c) tautype = 3 if the isolated track is not identified and had no surrounding neutrals

   (d) tautype = 4 if the isolated track is not identified and had one or more surrounding neutrals

5. **Narrow tau jet**

   If a narrow tau jet is found, its energy spread (angle that contains 75% of the jet energy) could not be bigger than 10°. The same requirements on azimuthal angles and aplanarities are imposed on the tau jet candidate as on a single isolated track. After a search for the charged track with the biggest energy in the tau jet, all charged and neutral tracks surrounding it in a cone of 15° are searched for. All the energies of these particles are added to the energy of the 'main' tau track. This energy has to exceed 5 GeV, while its product with the isolation angle of the tau jet has to be bigger than 150°GeV. Again a classification is made:

   (a) tautype = 3 if only one charged track and no neutral tracks are surrounding the main track

   (b) tautype = 4 if only one charged track and one or more neutrals are surrounding the main track

   (c) tautype = 5 if three charged tracks and no neutrals are surrounding the main track

   (d) tautype = 6 in all other cases

6. **Neural network inputs for tau events**

   For all categories of tau events the same 14 neural network inputs are chosen:

   (a) the thrust value of the event;

   (b) the polar angle of the hadronic di-jet system;

(c) the angle between the lepton and the hadronic W in the rest frame of the hadronic W;

(d) the angle between the 2 hadronic jets;

(e) the azimuthal angle between the 2 hadronic jets;

(f) the minimum angle between the lepton or leptonic jet and the 2 hadronic jets;

(g) the energy of the lepton and its surrounding particles in a cone of 15°.

(h) $|\cos(\theta_{\mathrm{miss}})|$;

(i) the category to which the tau event is classified;

(j) the total transverse momentum;

(k) the angle between the lepton or leptonic jet and the combined di-jet momentum;

(l) the effective centre of mass energy $\sqrt{s'}$;

(m) the isolation angle of the lepton or leptonic jet;

(n) the angle between the lepton or leptonic jet and the hadronic event plane.

The final neural network output is required to be bigger than 0.9, while only tau events of category 1 to 3 are used in the analysis. All numbers concerning the semi-leptonic events are summarised in Table 2.

References

[1] G. Goldhaber et al., Phys. Rev. Lett. **3** (1960) 181.

[2] R. Hanbury-Brown and R.Q. Twiss, Nature **178** (1956) 1046.

[3] T. Sjöstrand et al., *High-energy-physics event generation with PYTHIA 6.1,* Comp. Phys. Comm. **135** (2001) 238.

[4] L. Lönnblad and T. Sjöstrand, Eur. Phys. J. **C2** (1998) 165.

[5] L. Lönnblad and T. Sjöstrand, Phys. Lett. **B351** (1995) 293.

[6] OPAL Coll., G. Abbiendi et al., Eur. Phys. J. **C8** (1999) 559.

[7] ALEPH Coll., R. Barate et al., Phys. Lett. **B478** (2000) 50.

[8] L3 Coll., M. Acciarri et al., Phys. Lett. **B493** (2000) 233.

[9] S.V. Chekanov, E.A. De Wolf and W. Kittel, Eur. Phys. J. **C6** (1999) 403.

[10] DELPHI Coll., P. Aarnio et al., Nucl. Instr. and Meth. **A303** (1991) 233.

[11] DELPHI Coll., P. Abreu et al., Nucl. Instr. and Meth. **A378** (1996) 57.

[12] E.A. De Wolf, *Correlations in $e^+e^- \to W^+W^-$ hadronic decays,* hep-ph/0101243.

[13] C. Peterson, T. Rognvaldsson and L. Lonnblad, Comp. Phys. Comm. **81** (1994) 185.

[14] DELPHI Coll., P. Abreu et al., Phys. Lett. **B479** (2000) 89.

[15] J. Schwindling, B. Mansouié and O. Couet,
MLPFIT, http://home.cern.ch/schwing/MLPfit.html.

[16] A. De Angelis and L. Vitale, Nucl. Instr. and Meth. **A423** (1999) 446.

[17] V. Perevoztchikov, M. Tabidze and A. Tomaradze, *Influence of the bin-to-bin and inside-bin correlations on measured quantities,* DELPHI 2000 - 027 CONF 346.

[18] A.C. Davison and D.V. Hinkley, *Bootstrap Methods and Their Application,* Cambridge Univ. Pr. (1997).

[19] S. Catani et al., Phys. Lett. **B269** (1991) 432.

[20] G.C. Fox and S. Wolfram, Phys. Rev. Lett. **41** (1978) 1581.

[21] P. Abreu et al., *Correlations between particles in $e^+e^- \to W^+W^-$ events,* DELPHI 2000 - 115 Osaka CONF 414, Contributed paper to ICHEP 2000, Osaka, Japan.

[22] D. Morgan and M.R. Pennington, *Low energy $\pi\pi$ scattering,* in "The second DAPHNE Physics Handbook", ed. L. Maiani et al., 1995, pp. 193.

[23] G. Lafferty, Z. Phys. **C60** (1993) 659.

[24] G. Alexander and H. Lipkin, Phys. Lett. **B456** (1999) 270.

[25] P. Acton et al., (OPAL Coll.), Z. Phys. **C56** (1992) 521.

[26] P. Abreu et al., (DELPHI Coll.), Z. Phys. **C63** (1994) 17.

[27] P. Abreu et al., (DELPHI Coll.), Z. Phys. **C65** (1995) 587.

[28] D. Busculic et al., (ALEPH Coll.), Z. Phys. **C69** (1996) 379.

[29] P. Abreu et al., (DELPHI Coll.), Phys. Lett. **B355** (1995) 415.

[30] S. Todorova-Nova et al., *Particle correlations in* $e^+e^- \to W^+W^-$ *events with the DELPHI detector,* DELPHI 2001 - 107 CONF 534, Contributed paper to Moriond 2001.

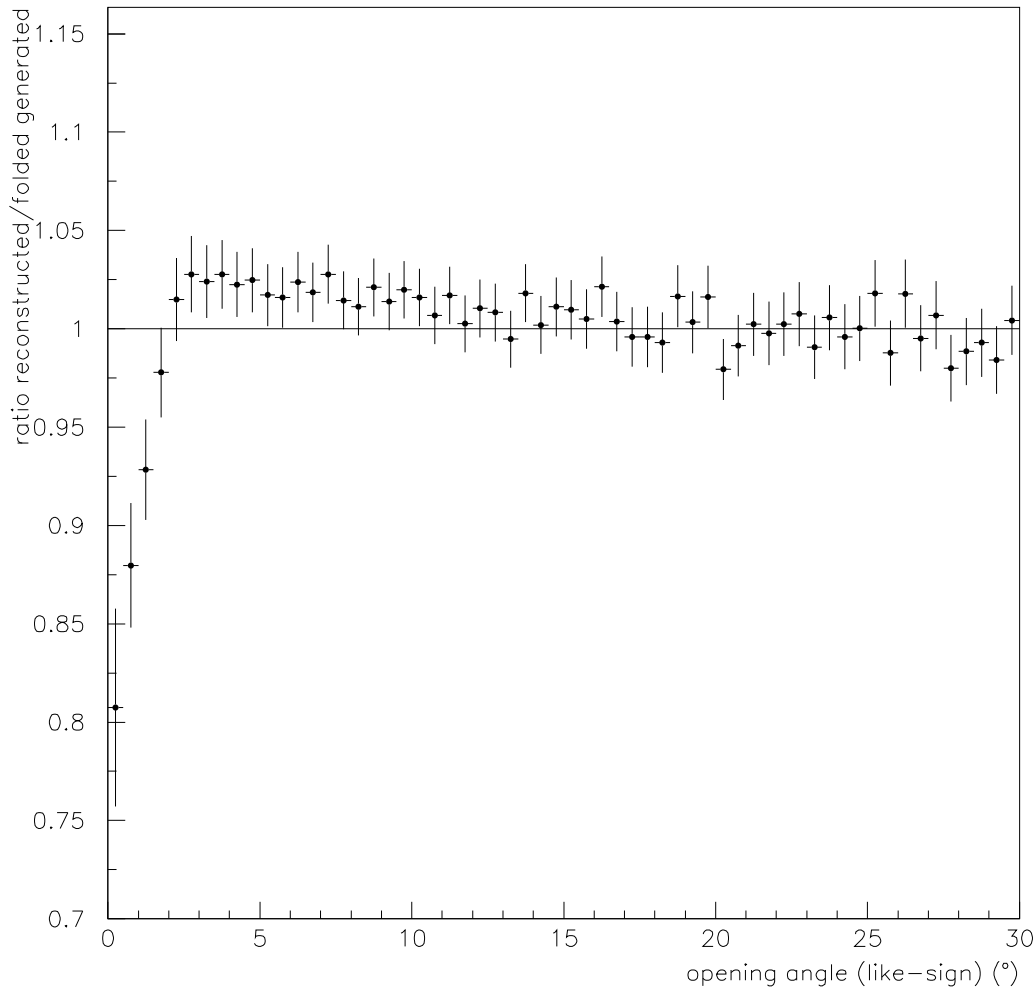

Figure 1: Reconstruction efficiency for like-sign pairs as a function of the opening angle α between the particles of the pair.

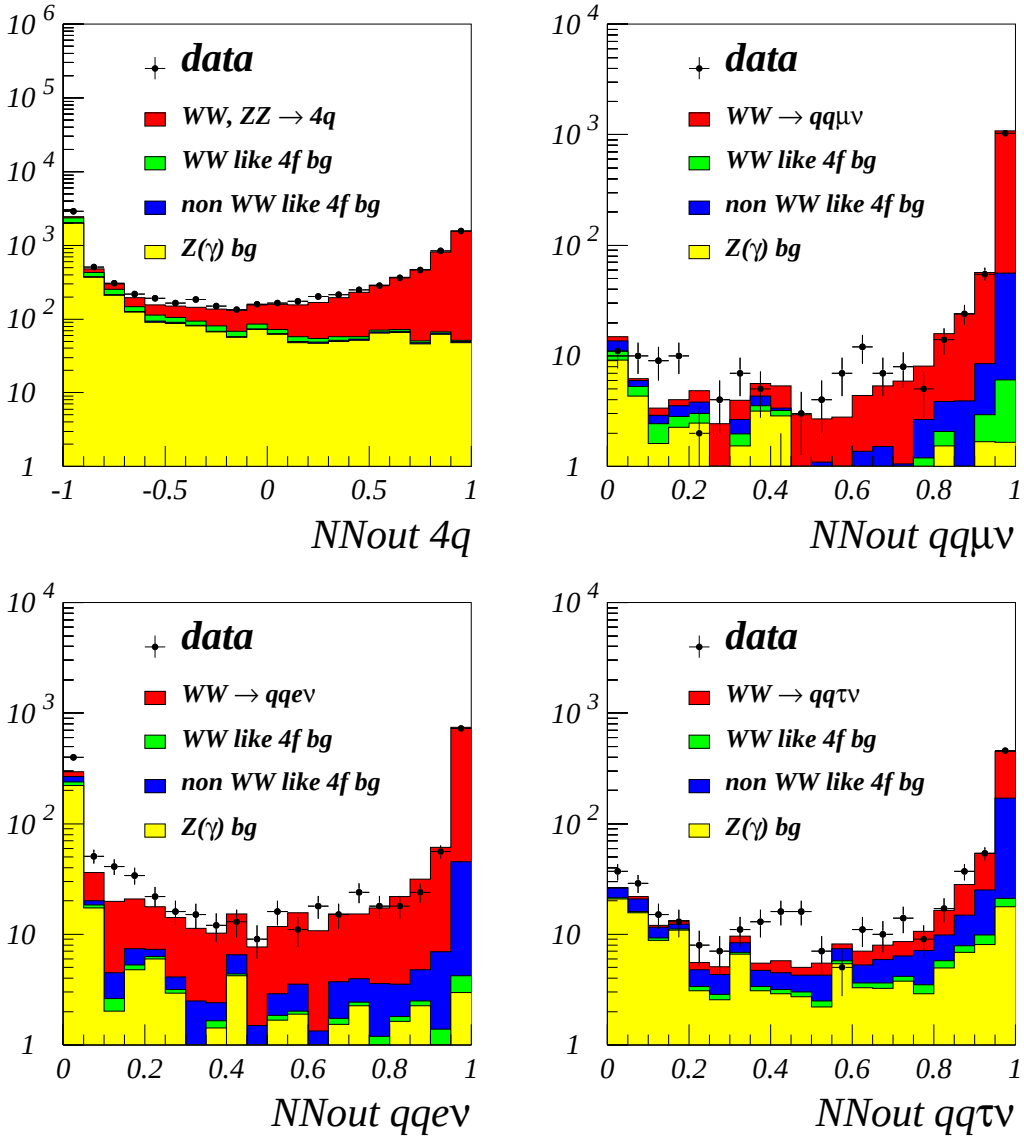

Figure 2: The neural network output distributions for all four selections using the combined data set, compared with simulation predictions.

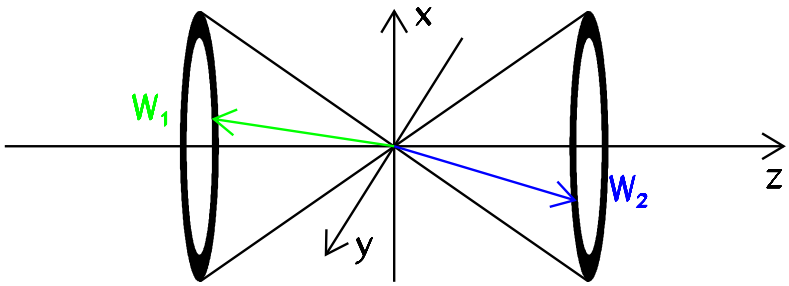

Figure 3: The surface on which different single W systems can be combined into a fully hadronic mixed event.

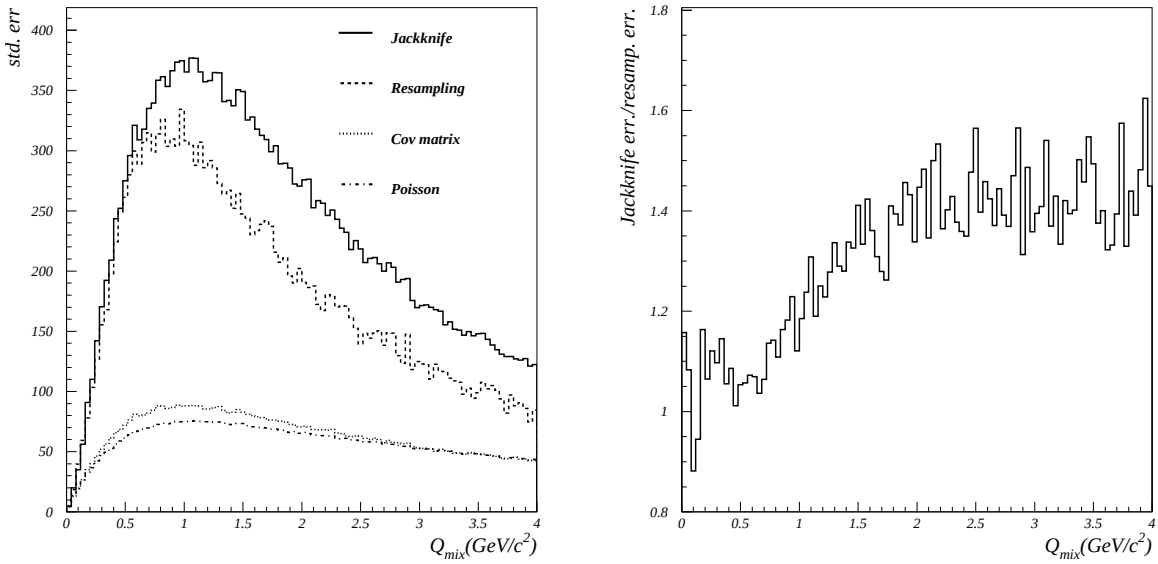

Figure 4: Different error estimates for the $\rho_{mix}^{WW}(Q)$ distribution (left) and the ratio of the error estimated using the Jackknife method w.r.t. resampling (right).

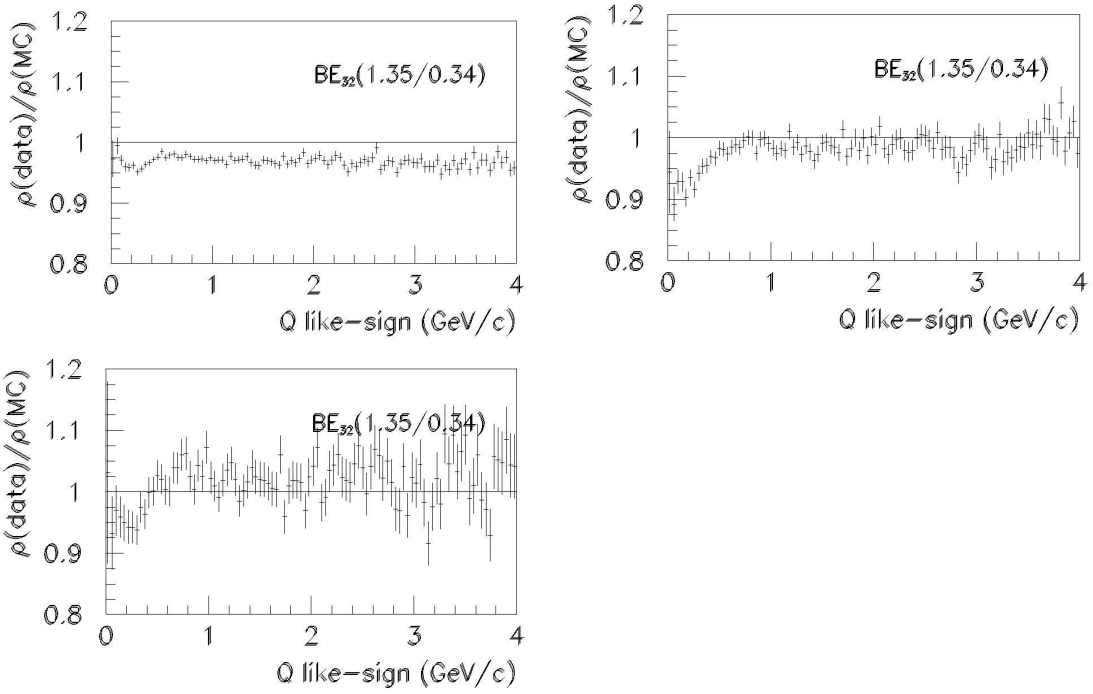

Figure 5: The ratio of the two-particle densities for Z^0 events in data and in Monte Carlo events with BEC, with parameters λ=1.35 and r=0.34, for the inclusive ($4q$) sample, with a cut on $d_{join} > 4$ GeV/c and $d_{join} > 6.5$ GeV/c.

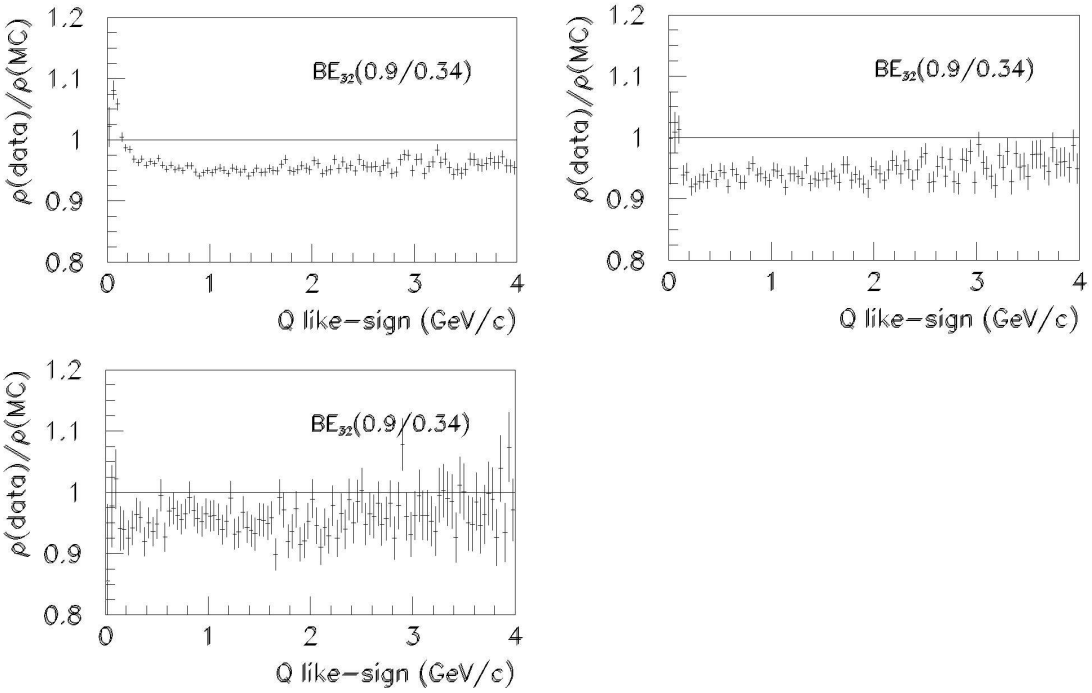

Figure 6: As in Fig. 4 but with λ=0.9.

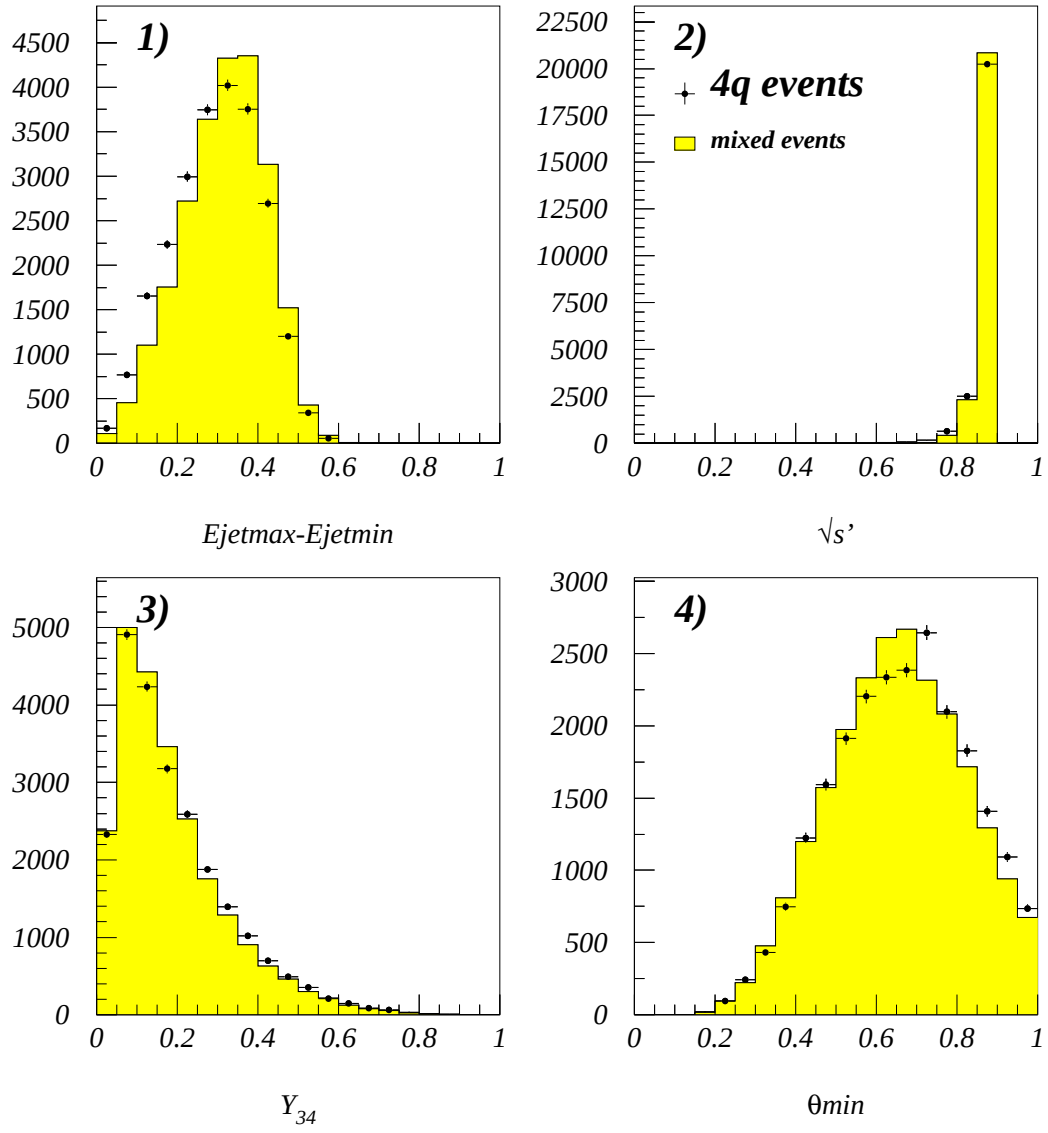

Figure 7: Comparison of the neural network input variables (numbered 1 to 13 in section 7.2.1) between the Monte Carlo ($4q$) sample (full dots) and the mixed sample (histogram) on this and the next four pages. The quantities on the x-axis are normalized to the interval (0., 1.). Five extra quantities, also described in section 9.1, are also displayed.

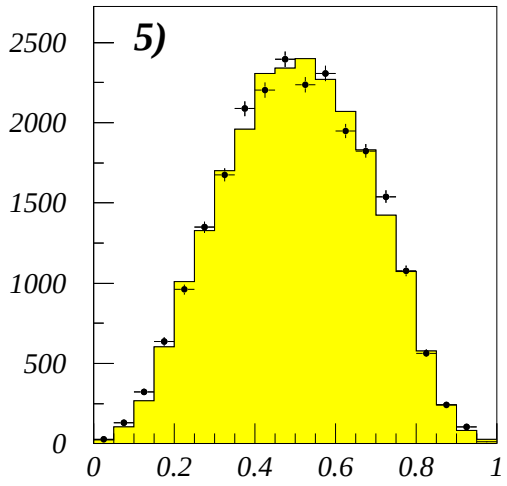

sph

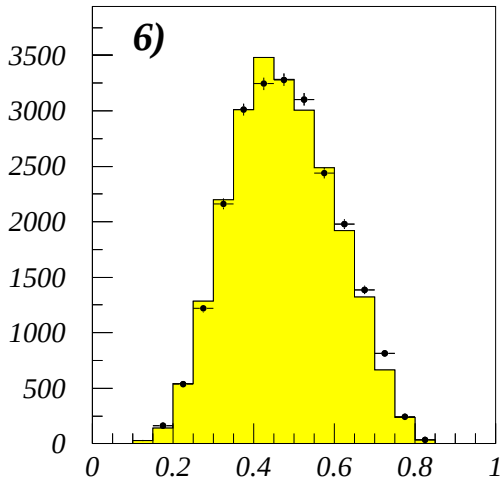

thrust

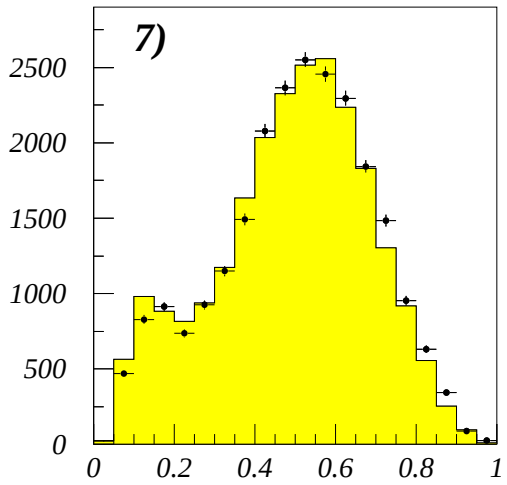

bmin

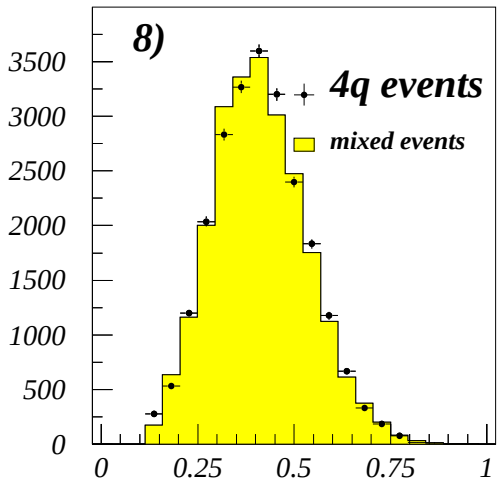

nminj

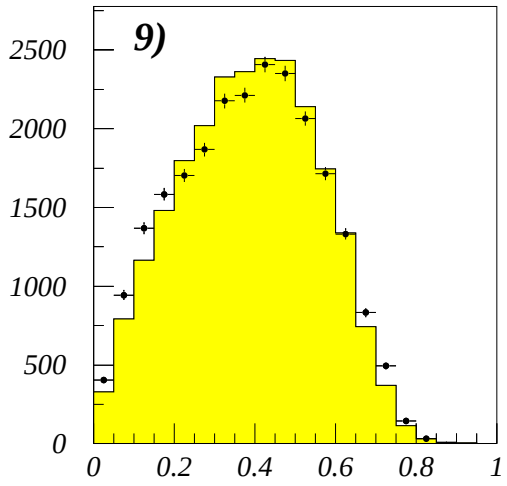

H3

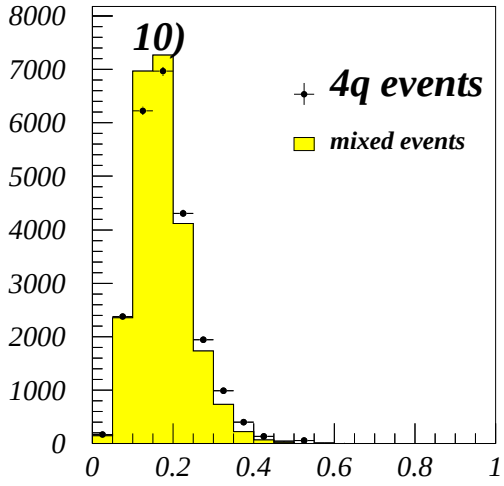

H4

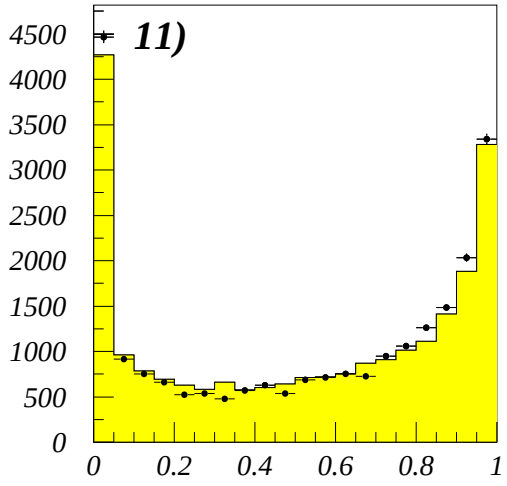

probww

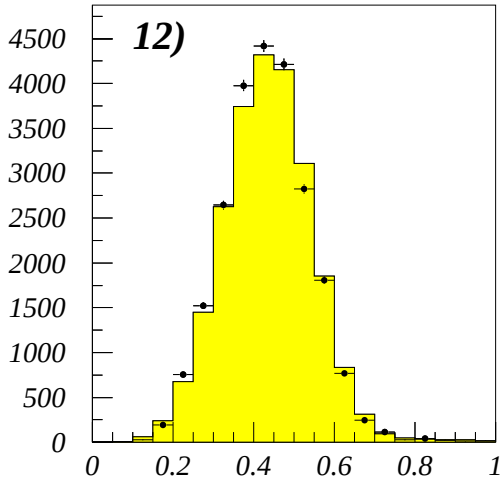

E_{trans}

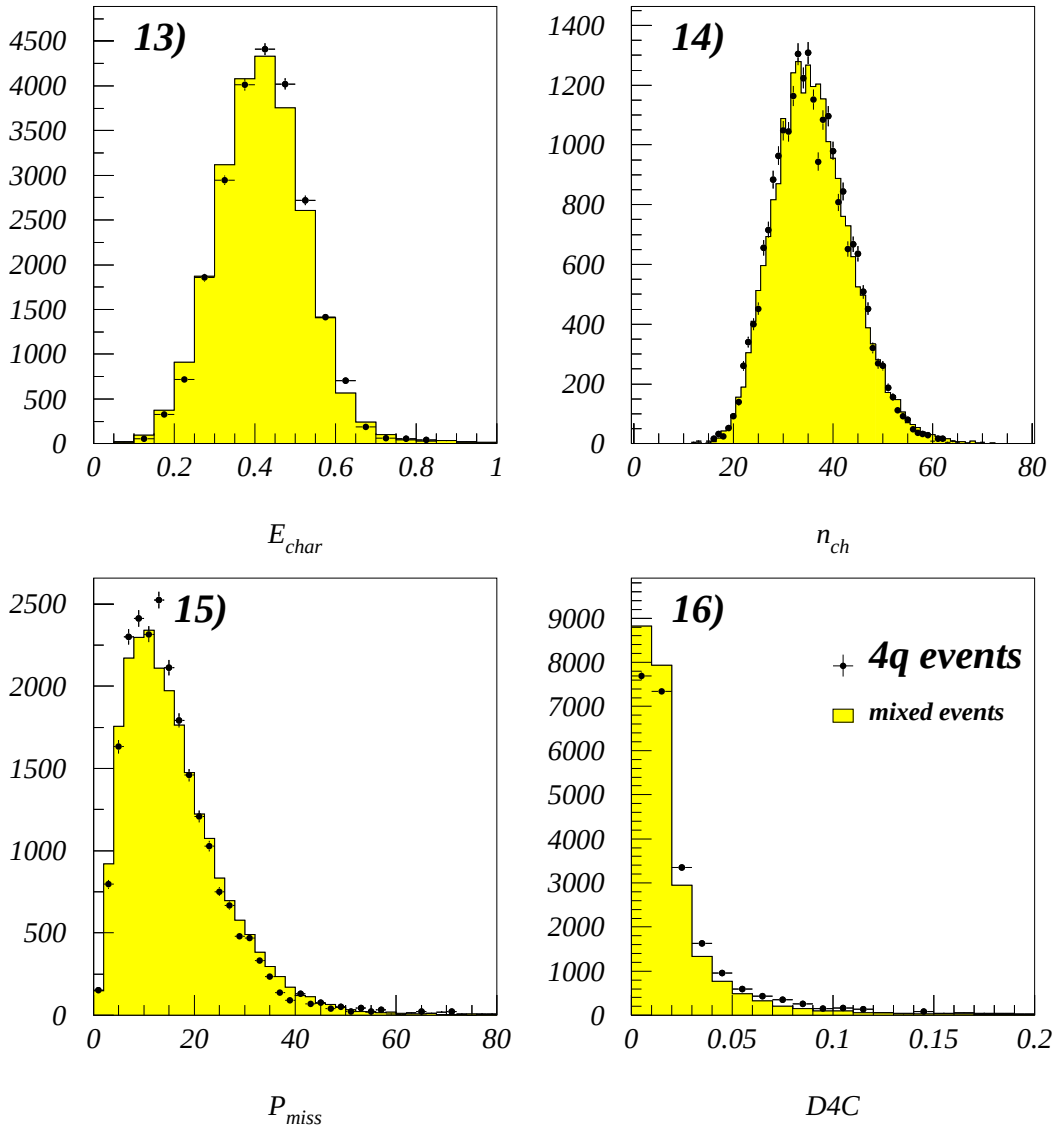
13)
4500
4000
3500
3000
2500
2000
1500
1000
500
0
0
0.2
0.4
0.6
0.8
1
E_{char}
14)
1400
1200
1000
800
600
400
200
0
0
20
40
60
80
n_{ch}
15)
2500
2000
1500
1000
500
0
0
20
40
60
80
P_{miss}
16)
4q events
mixed events
9000
8000
7000
6000
5000
4000
3000
2000
1000
0
0
0.05
0.1
0.15
0.2
D4C

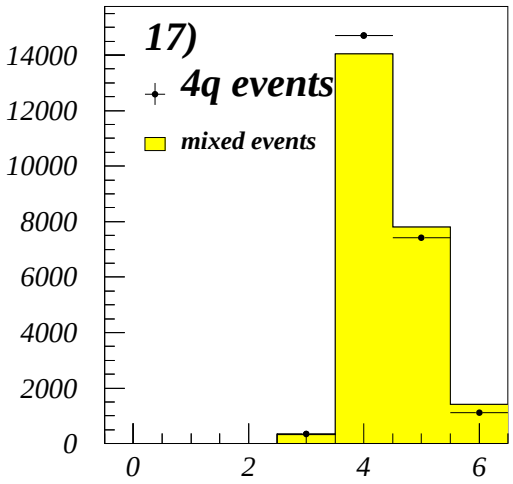
17)
4q events
mixed events
14000
12000
10000
8000
6000
4000
2000
0
0
2
4
6
nr of jets

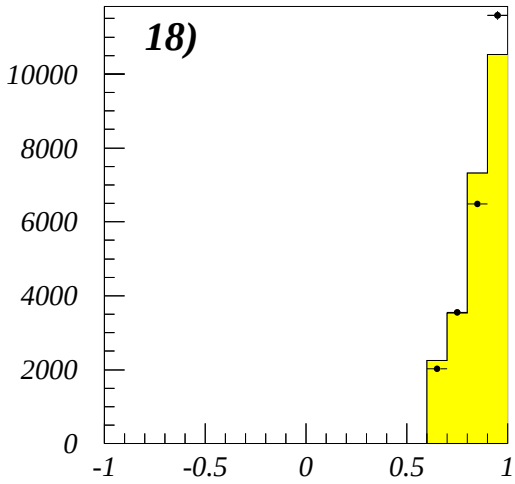
18)
10000
8000
6000
4000
2000
0
-1
-0.5
0
0.5
1
nnout 4q

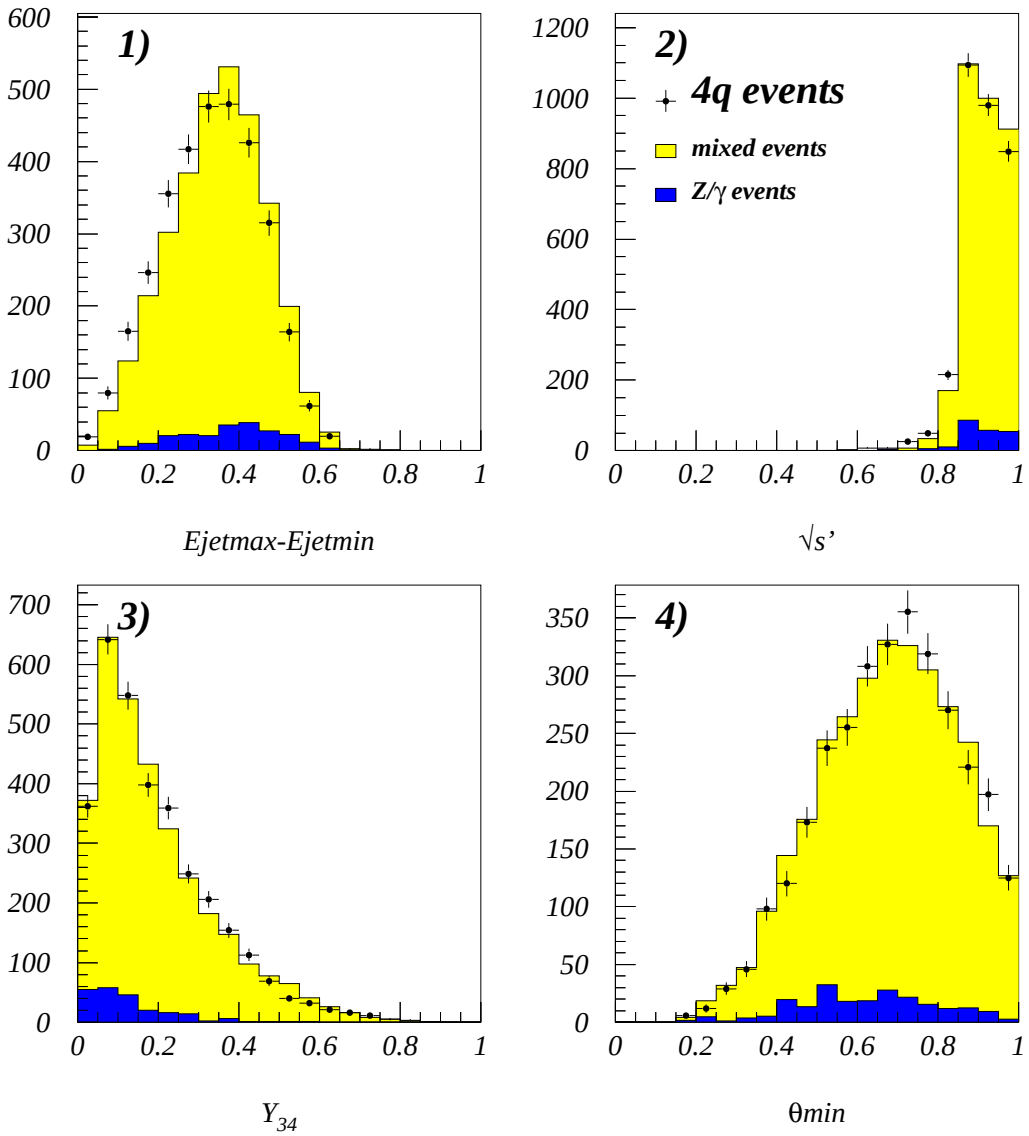

Figure 8: Same as in previous figure with the real ($4q$) combined data (full points), the mixed events (histogram) and background (dark coloured) on thi and the next four pages.

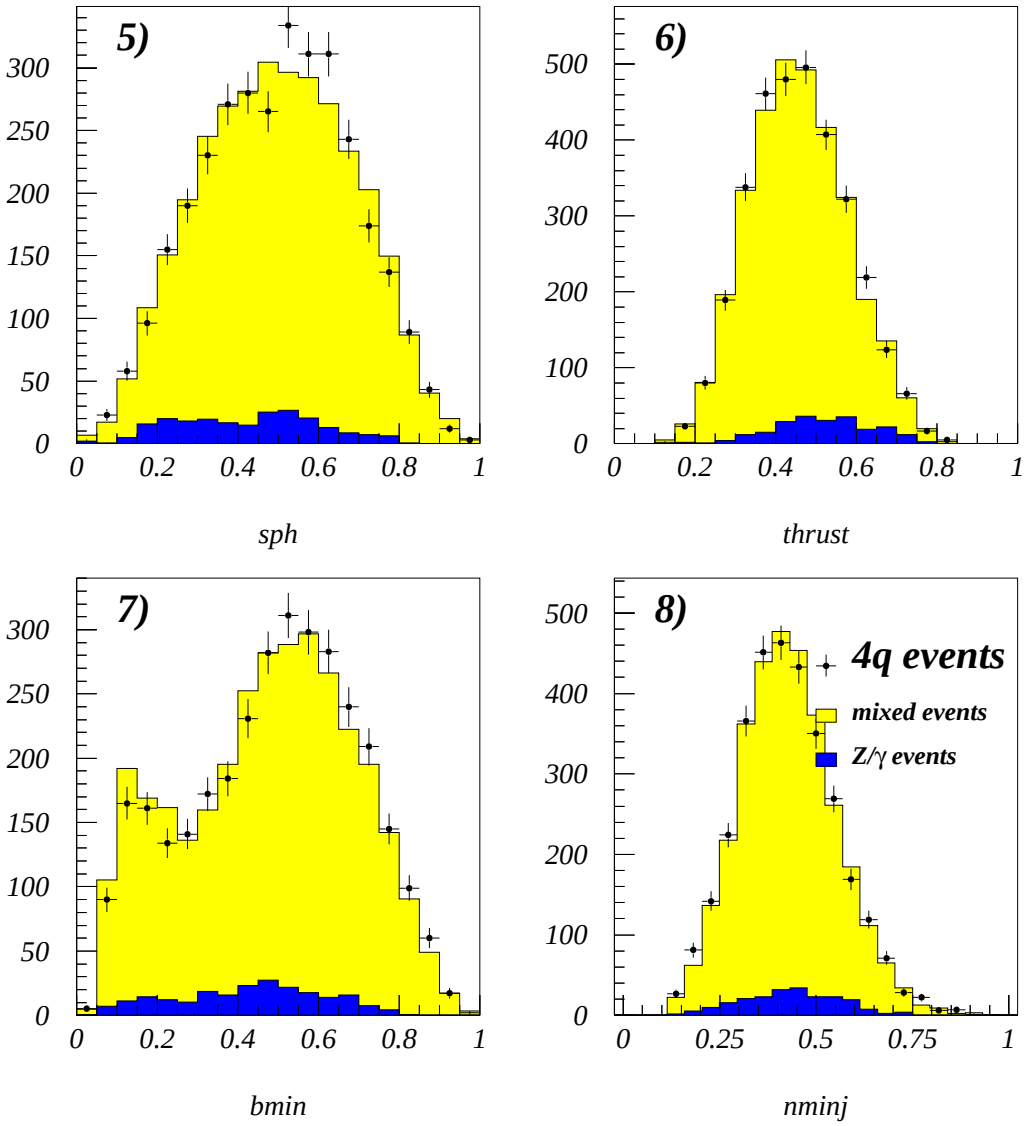
5)
sph
6)
thrust
7)
bmin
8)
4q events
mixed events
Z/γ events
nminj

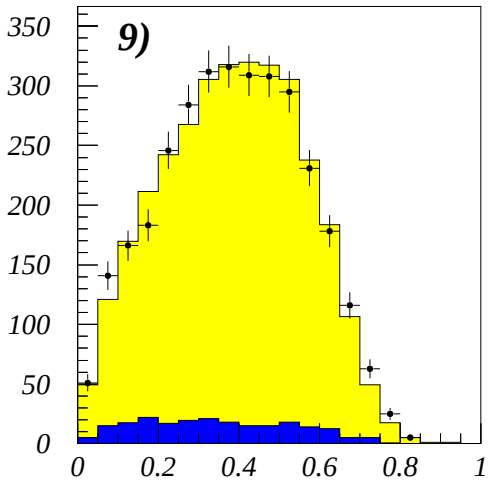

H3

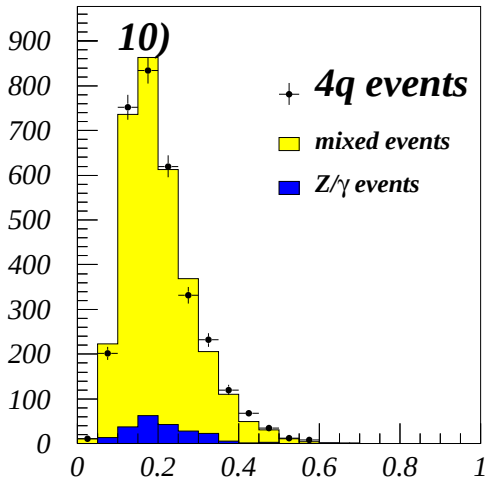

H4

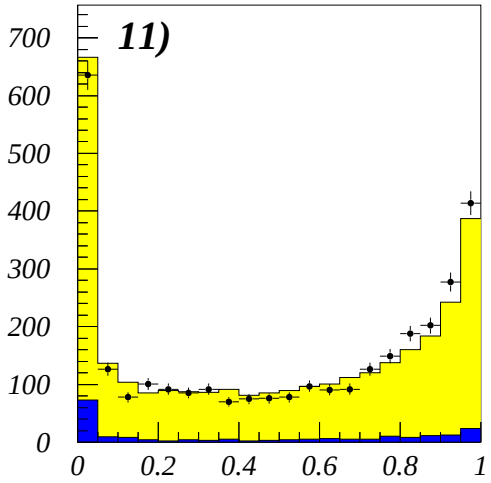

probww

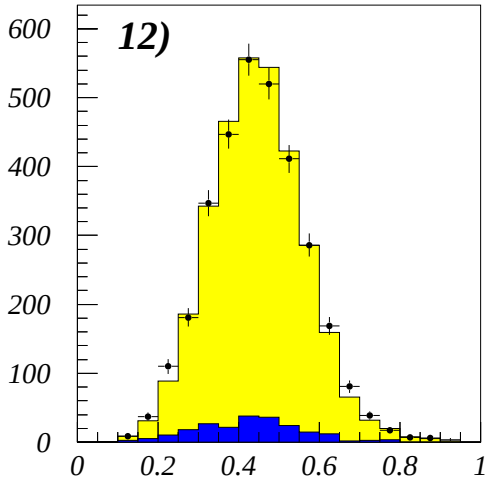

E_{trans}

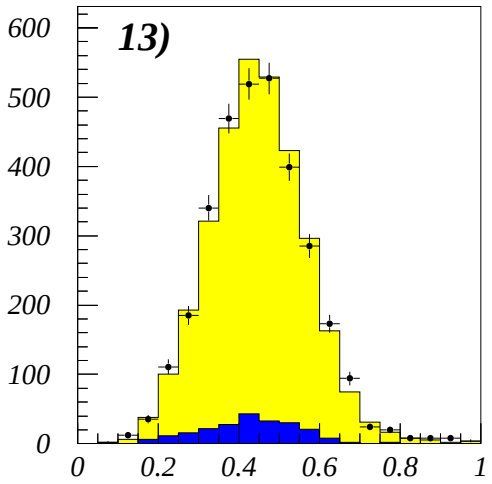
13)
600
500
400
300
200
100
0
0
0.2
0.4
0.6
0.8
1
E_{char}

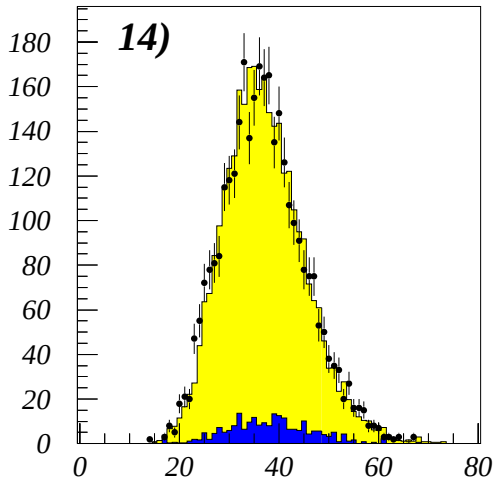
14)
180
160
140
120
100
80
60
40
20
0
0
20
40
60
80
n_{ch}

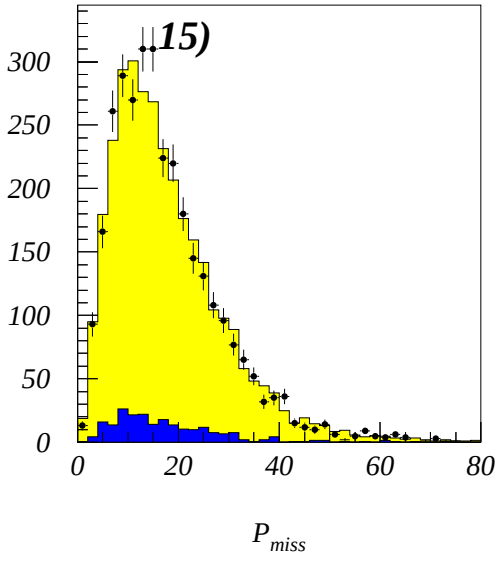
15)
300
250
200
150
100
50
0
0
20
40
60
80
P_{miss}

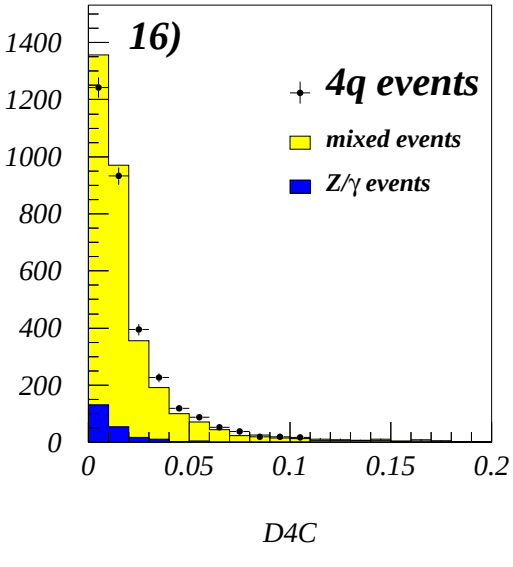
16)
4q events
mixed events
Z/γ events
1400
1200
1000
800
600
400
200
0
0
0.05
0.1
0.15
0.2
D4C

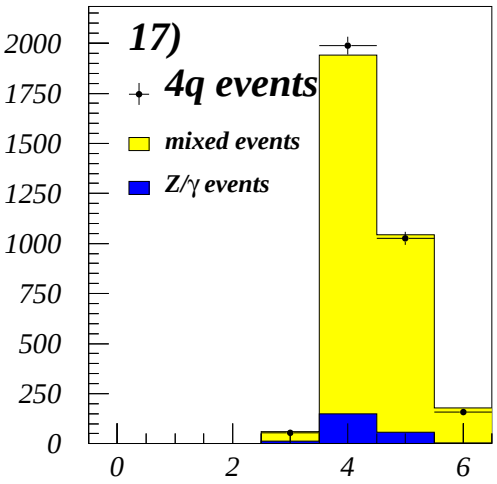

nr of jets

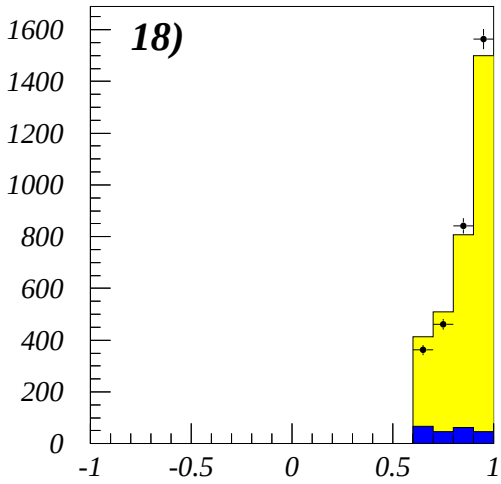

nnout 4q

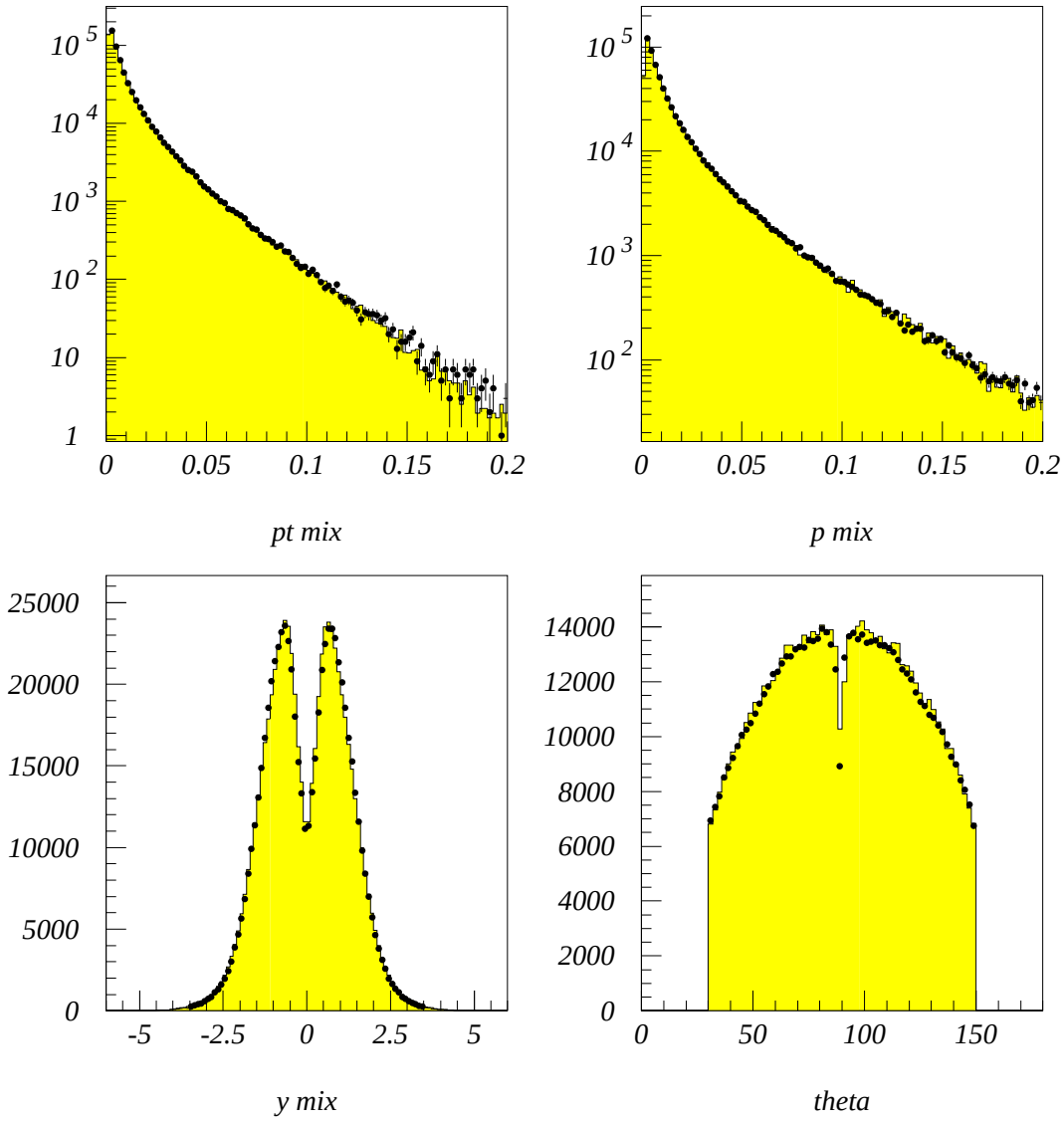

Figure 9: Distribution of the transverse momentum, the momentum, rapidity and polar angle of Monte Carlo events in ($4q$) events (data points) and mixed events (histogram).

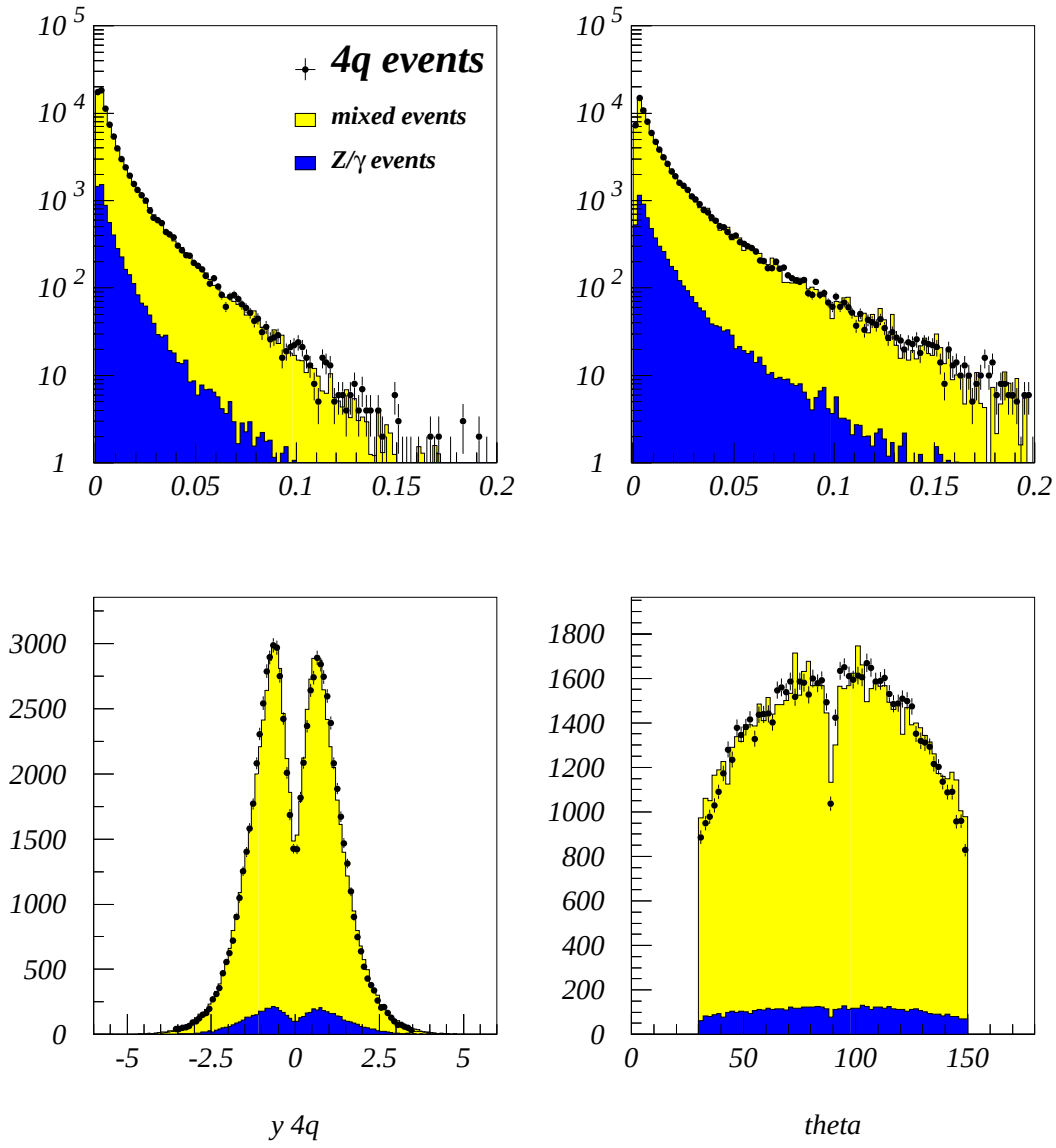

Figure 10: As in previous figure for real ($4q$) events and mixed events.

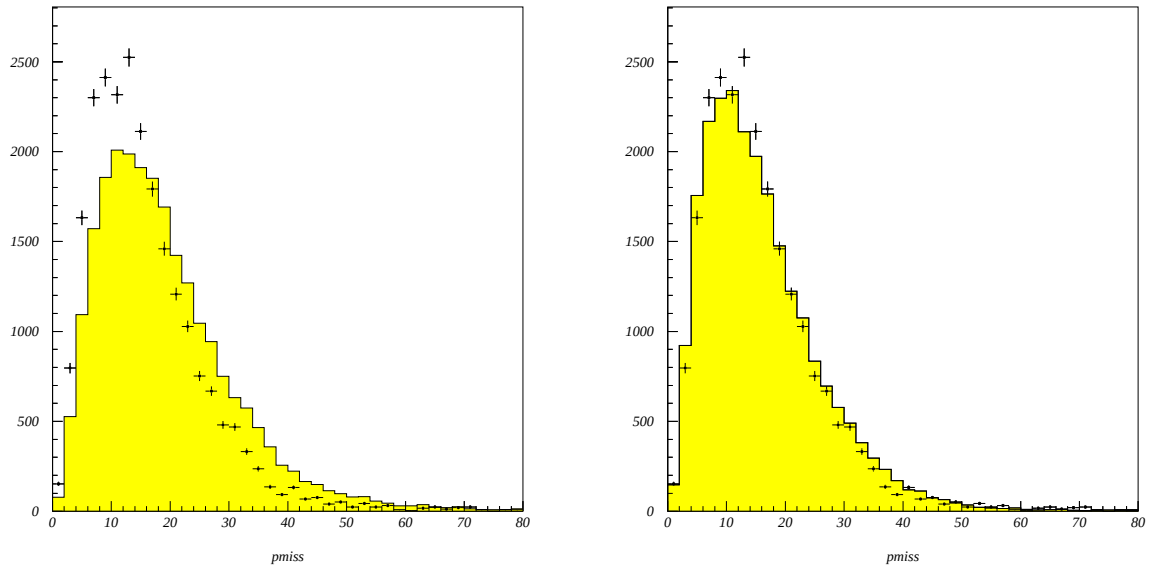

Figure 11: Effect of W momentum smearing on the missing momentum distribution.

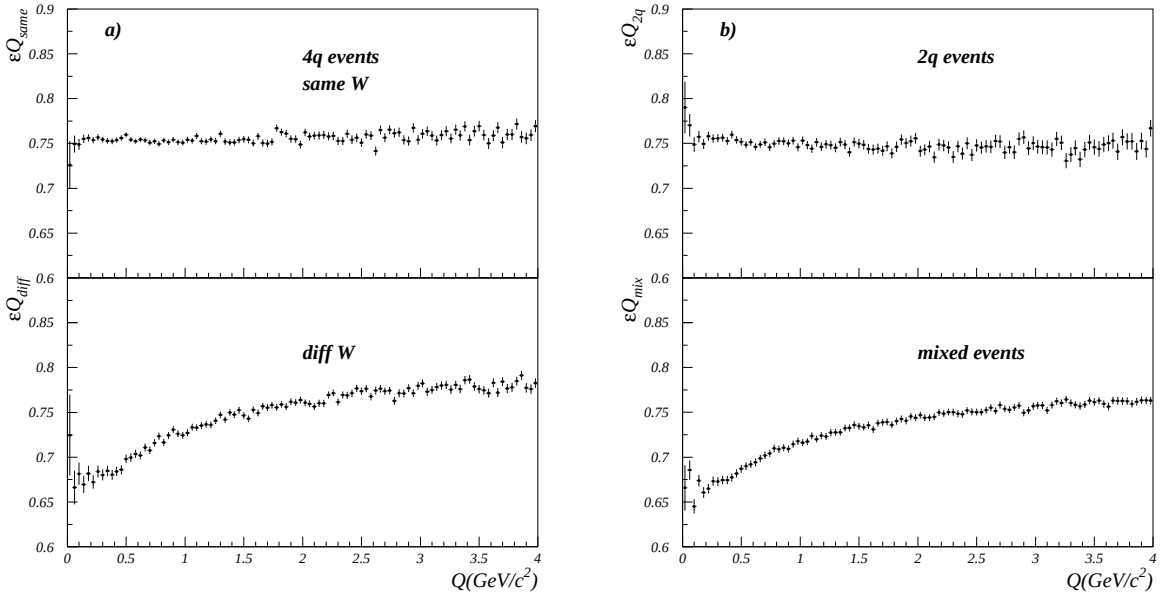

Figure 12: Selection efficiencies of the two-particle spectra as a function of Q.

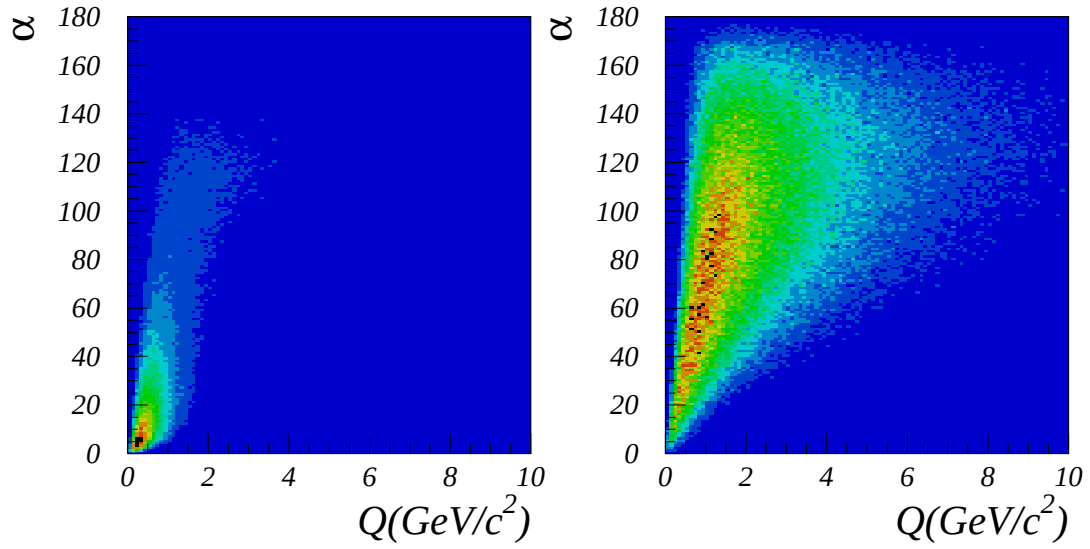

Figure 13: Two-particle density as function of Qvariable and the opening angle α between a pair of particles for particles from the *same* W (left) or from *different* W's (right).

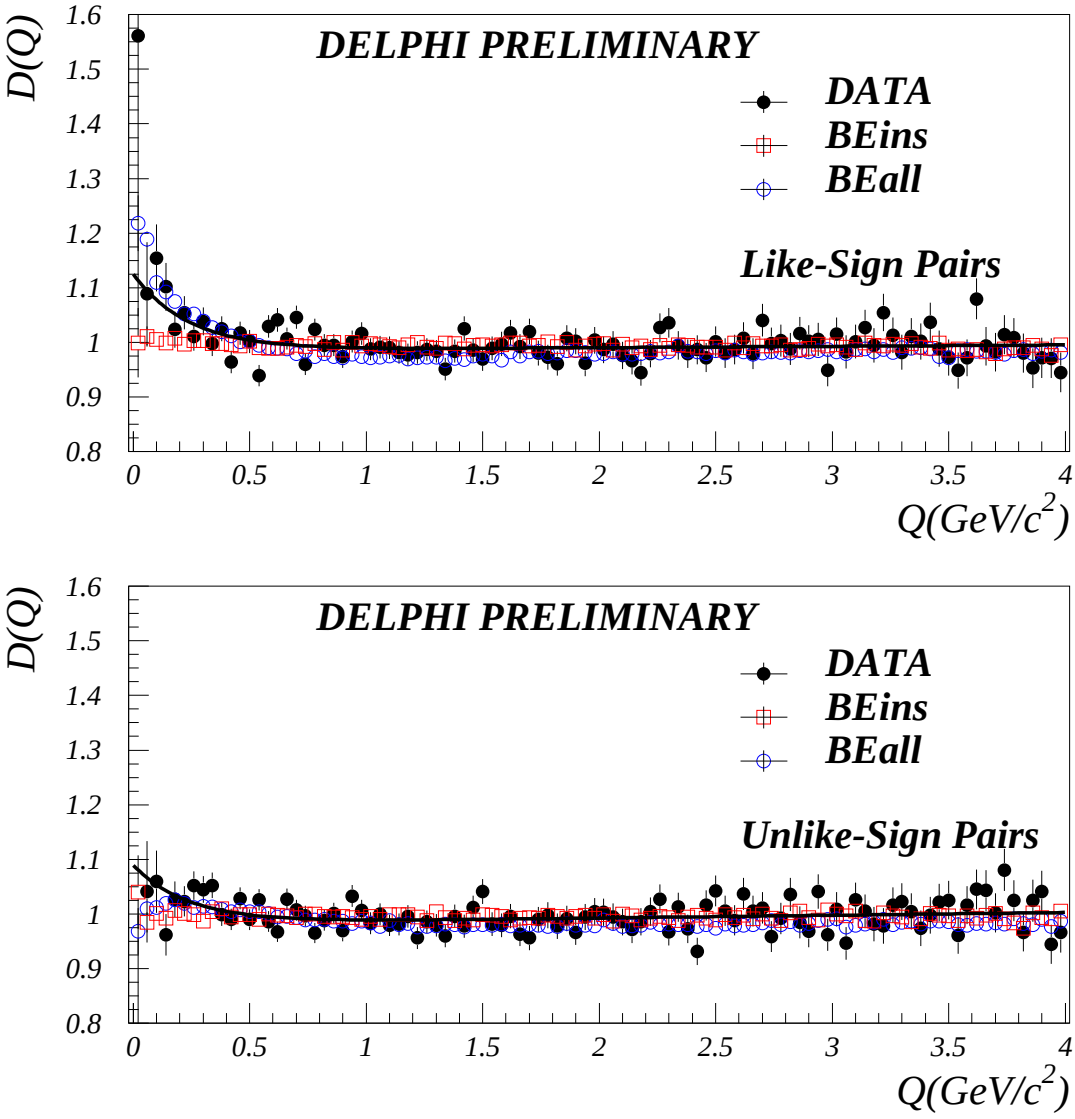

Figure 14: Comparison of the $D(Q)$ variable for the combined data set with MC model predictions BEins and BEall (i.e. the same as BEfull) for like-sign particle pairs (top) and unlike-sign particle pairs (bottom).

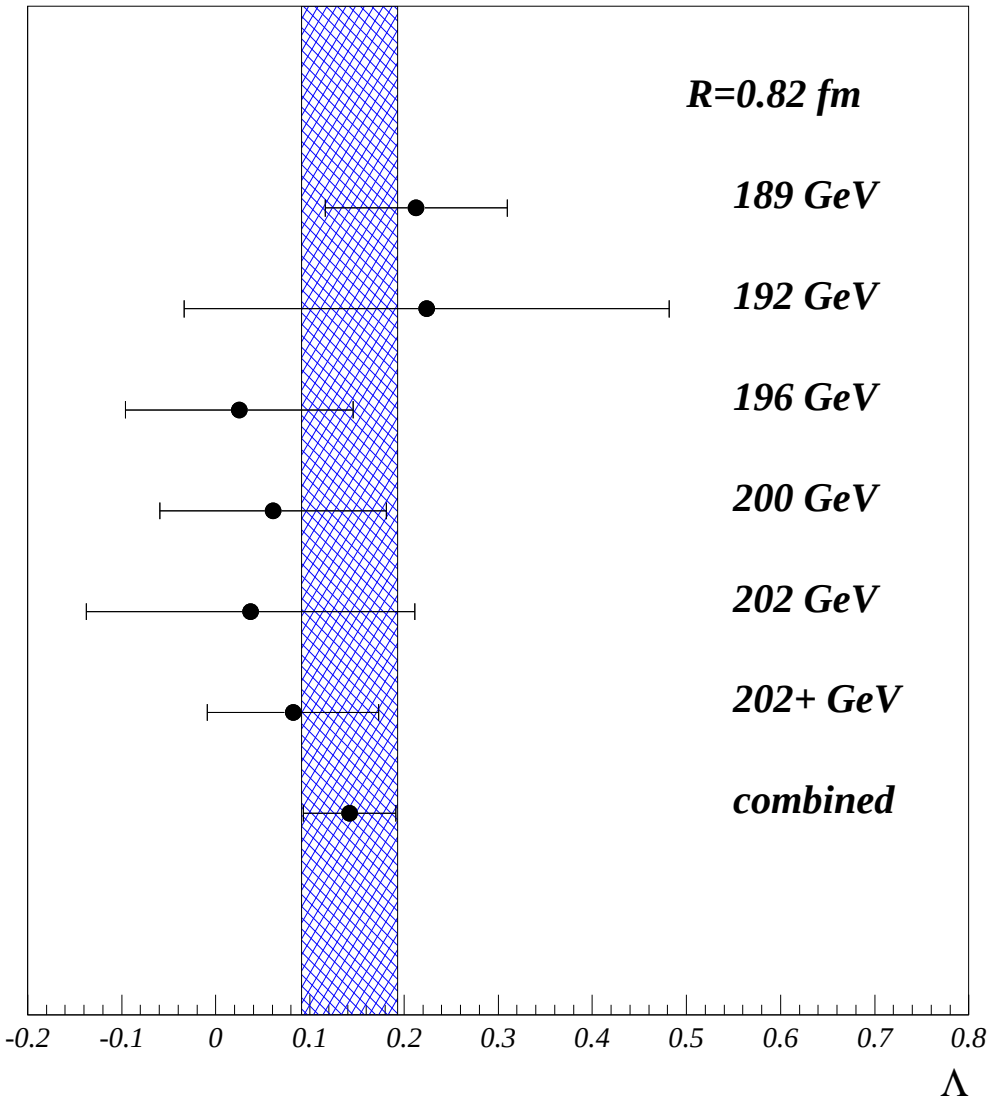

Figure 15: An overview of the fitted Λ-parameter for like-sign particle pairs for all analysed energies, fixing the radius to 0.82 fm.

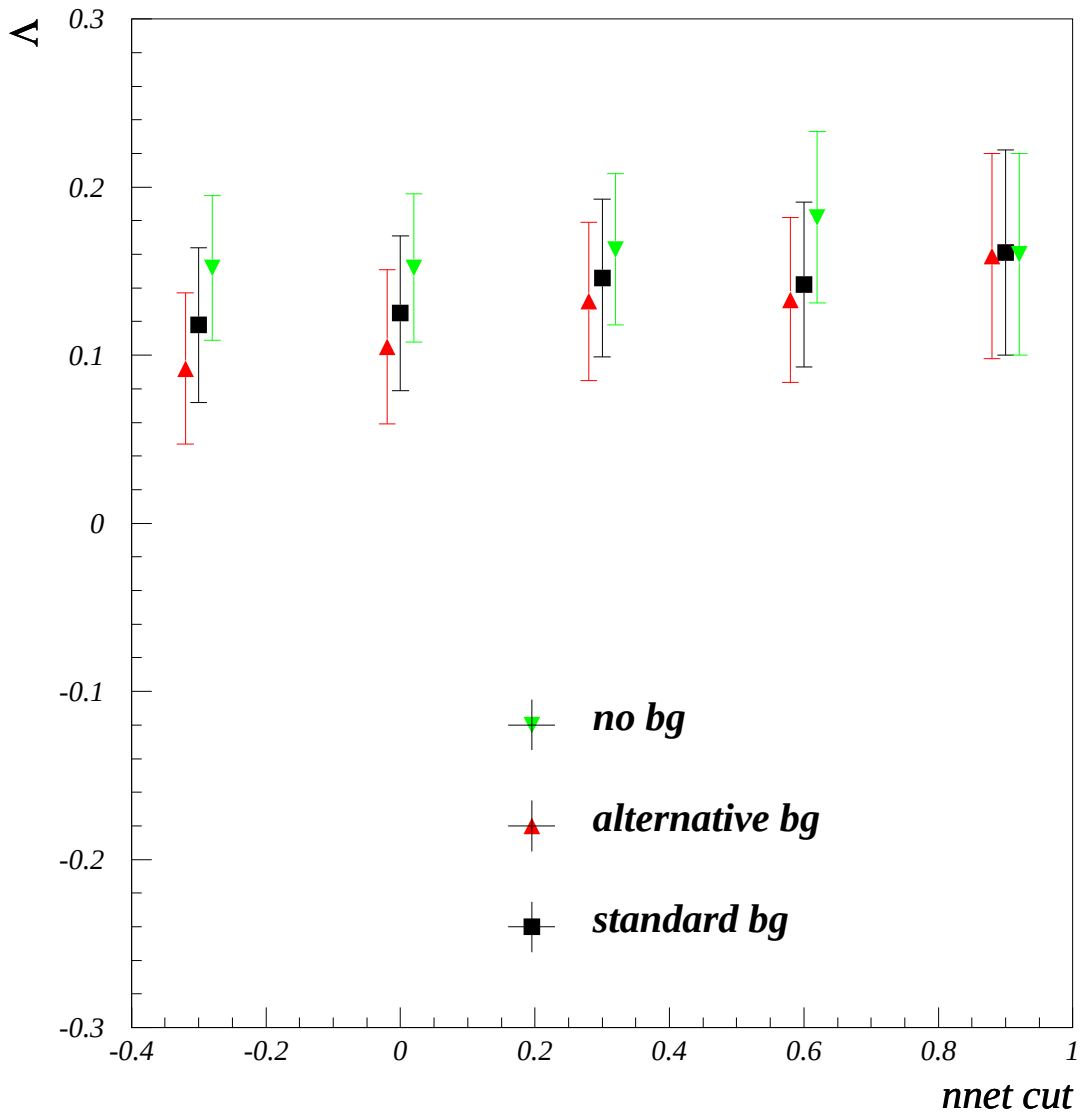

Figure 16: An overview of the fitted Λ parameter for like-sign particle pairs for different cuts on the neural network output parameter, and thus purity of the sample, fixing the radius to 0.75 fm.

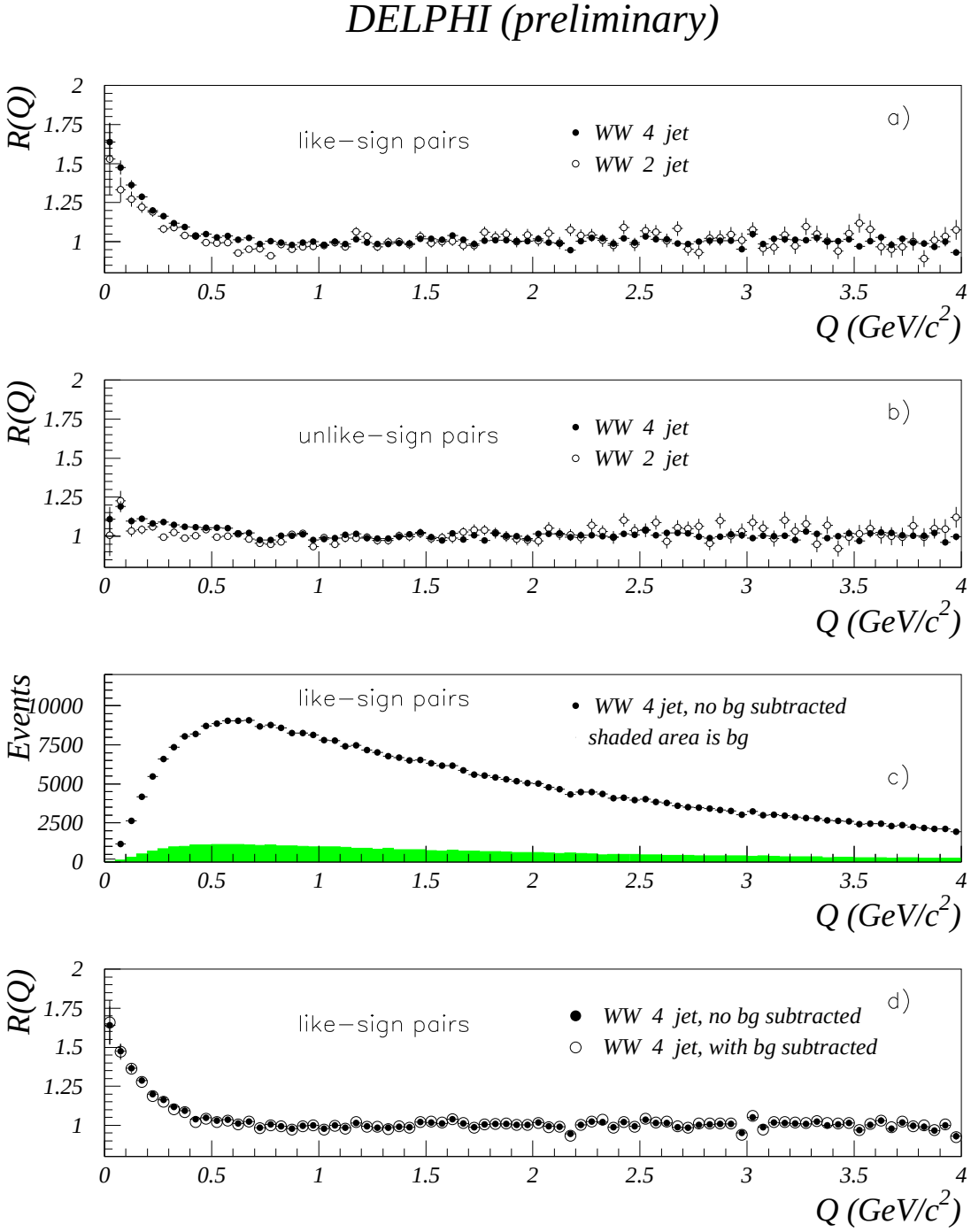

Figure 17: (a) Measured correlation functions $R_{2q}(Q)$ (open circles) and $R_{4q}(Q)$ (closed circles) for like-sign pairs. (b) same as (a) but for unlike-sign pairs. (c) Q-distributions for real (4q) events (closed circles) and for simulated (4q) background events (shaded area) for like-sign particle pairs. (d) measured $R_{4q}(Q)$ distributions for (4q) before and after background subtraction (closed and open circles, respectively).

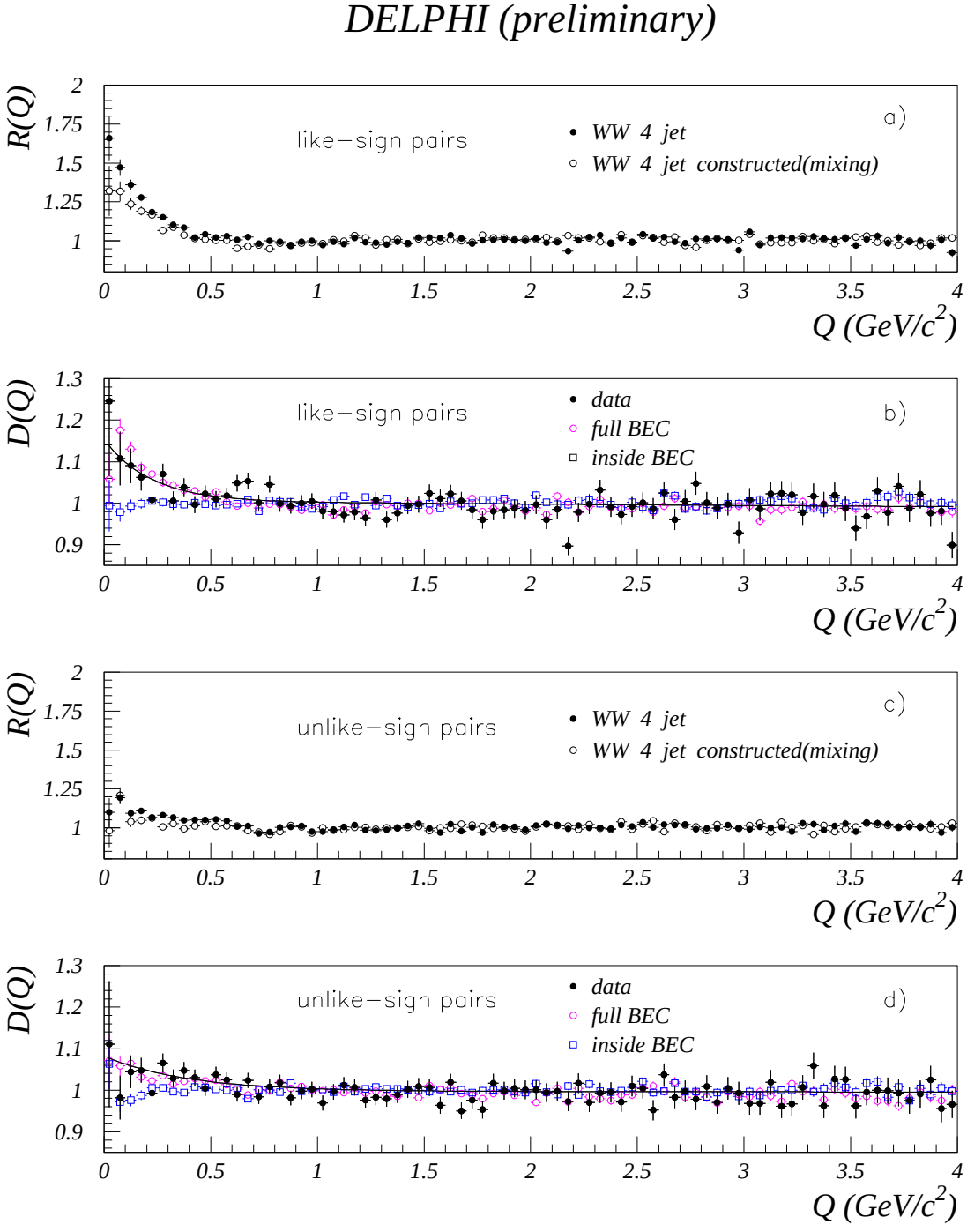

Figure 18: (a) Measured correlation functions $R_{4q}(Q)$ (closed circles) and $R_{4q}(Q)(constructed)$ (open circles) for like–sign particle pairs computed from (2q) events using the mixing technique. (b) The ratio $D(Q)$ of fully hadronic to mixed events for like–sign particle pairs for data, for full BEC and for inside BEC. (c) same as (a) but for unlike–sign pairs. (d) same as (b) but for unlike–sign pairs.